Using a Scenario-Neutral Framework to Avoid Potential Maladaptation to Future Flood Risk

Ciaran Broderick[1] iD **, Conor Murphy[1]** iD **, Robert L. Wilby[2]** iD **, Tom Matthews[2],
Christel Prudhomme[2,3], and Mark Adamson[4]**

[1]Irish Climate Analysis and Research UnitS (ICARUS), Department of Geography, Maynooth University, Maynooth, Ireland, [2]Department of Geography, Loughborough University, Loughborough, UK, [3]European Centre for Medium-Range Weather Forecasts, Reading, UK, [4]Flood Relief and Risk Management Division, Office of Public Works, Trim, Ireland

Abstract This study develops a coherent framework to detect those catchment types associated with a high risk of maladaptation to future flood risk. Using the "scenario-neutral" approach to impact assessment the sensitivity of Irish catchments to fluvial flooding is examined in the context of national climate change allowances. A predefined sensitivity domain is used to quantify flood responses to +2 °C mean annual temperature with incremental changes in the seasonality and mean of the annual precipitation cycle. The magnitude of the 20-year flood is simulated at each increment using two rainfall-runoff models (GR4J, NAM), then concatenated as response surfaces for 35 sample catchments. A typology of catchment sensitivity is developed using clustering and discriminant analysis of physical attributes. The same attributes are used to classify 215 ungauged/data-sparse catchments. To address possible redundancies, the exposure of different catchment types to projected climate is established using an objectively selected subset of the Coupled Model Intercomparison Project Phase 5 ensemble. Hydrological model uncertainty is shown to significantly influence sensitivity and have a greater effect than ensemble bias. A national flood risk allowance of 20%, considering all 215 catchments is shown to afford protection against ~48% to 98% of the uncertainty in the Coupled Model Intercomparison Project Phase 5 subset (Representative Concentration Pathway 8.5; 2070–2099), irrespective of hydrological model and catchment type. However, results indicate that assuming a standard national or regional allowance could lead to local over/under adaptation. Herein, catchments with relatively less storage are sensitive to seasonal amplification in the annual cycle of precipitation and warrant special attention.

Plain Language Summary Climate change presents a significant challenge for flood managers. Their decisions regarding the designation of vulnerable areas and investment in large-scale flood prevention and relief schemes have long-term implications for the attendant risk to human life and infrastructure. In some jurisdictions authorities have proposed a universal allowance on existing design measures that would offer protection against a set (e.g., 20%) increase in flood magnitude. However, this "one size fits all" approach ignores that river catchments have very different physical attributes that affect their sensitivity to change. We develop a framework that groups catchments based on their physical characteristics into distinct sensitivity types. The method follows the "scenario-neutral" approach to impact assessment. Here two-dimensional response surfaces showing flood sensitivity to incremental changes in rainfall and temperature are used in conjunction with the latest climate projections to tailor climate plans for individual catchments. The response surfaces are a valuable tool for identifying critical thresholds when proposed allowances fail to accommodate projected flood risk. For managers this helps to allocate resources where risk is greatest and balance the costs of increased protection against climate uncertainty. The study is conducted using 215 Irish catchments; however, we highlight its potential to aid adaptation efforts globally.

1. Introduction

Climate change presents significant challenges for decision makers. Uncertainty about the exact trajectory of future change coupled with the complexity of hydrological processes means these difficulties are particularly acute in flood management, where robust decisions regarding the designation of at risk areas and investment in long-lived infrastructure are required. Some national authorities are designating flood risk allowances to factor climate change impacts and attendant analytical uncertainties into engineering

designs (DCLG, 2012; Löschner et al., 2017; Reynard et al., 2017). Authorities are also using allowances to investigate community vulnerability and to inform adaptive approaches to risk management (OPW, 2015). "Scenario-neutral" (SN) approaches are increasingly employed to evaluate these potential climate change impacts on water and environmental systems (Brown & Wilby, 2012; Bussi, Dadson, et al., 2016; Bussi, Whitehead, et al., 2016; Culley et al., 2016; Guo et al., 2017; Prudhomme et al., 2010, 2015; Vormoor et al., 2017; Whateley et al., 2014). SN approaches involve testing the responsiveness of a local indicator (e.g., reservoir levels) to incremental adjustments in key driving climate variables (e.g., temperature, rainfall), across a plausible range of changes in variable intensity and seasonality. This study uses a SN approach to assess the sensitivity of flood regimes and hence fitness of national design allowances to climate change. We demonstrate the analytical framework using a large set of Irish catchments that represent a range of hydrological conditions.

Although the amount of impact modeling required for a comprehensive sensitivity assessment may be substantial, the SN approach provides deep insight to a system's response to a wide range of climatic changes. Moreover, SN approaches overcome a key limitation of "scenario-led" (SL) analyses, which are typically constrained by available climate model projections and thereby may fail to test sensitivity to more extreme scenarios, even so-called "black swan" events. Nonlinearity in hydrological responses to climate variability and change (particularly for extreme events) further justifies the exploration of a wider spectrum of plausible conditions. In addition, by relying directly on GCM (Global Climate Model) projections to quantify local impacts, the SL approach is subject to biases/errors (e.g., climate model and system uncertainties) inherited through the modeling chain—thus requiring additional postprocessing and bias correction (Lin et al., 2017; Maraun et al., 2017; Smith et al., 2018; Wang et al., 2014). In contrast, within the SN approach GCM simulations are only used to provide guidance on the possible future risks.

The SN approach has several additional benefits. Similar to measures of elasticity it is shown to capture the complex nonlinear relationship between various indices of flow and climate (Andréassian et al., 2016; Chiew, 2006; Dooge et al., 1999; Fu et al., 2007; Sankarasubramanian et al., 2001; Singh et al., 2014). Furthermore, it can reveal which hydroclimatological variables most impact local systems and how antecedent conditions can influence sensitivity. Such information can help to refine management options (Guo et al., 2017; Prudhomme et al., 2010). The framework can also be adapted to examine the effect of different climate and hydrological model uncertainties (Kay, Crooks, & Reynard, 2014; Steinschneider, McCrary, et al., 2015; Steinschneider, Wi, et al., 2015) as well as other exogenous factors such as climate-related land cover changes (Yates et al., 2015).

The SN framework is a flexible decision-making tool (Brown et al., 2011; Poff et al., 2016; Turner et al., 2014; Weiß, 2011; Weiß & Alcamo, 2011; Yates et al., 2015). The method can pinpoint important tipping points or climatic thresholds at which the risk of system failure or impairment becomes significant. Similarly, it can highlight existing resilience; knowledge that is important for cost-effective adaptation (Brown et al., 2012, 2011). By mapping climate model projections onto the sensitivity domain, exposure to climate risk (as defined by current climate ensembles) can be established. Management plans can thus be updated using successive generations of model projections without undertaking additional impact modeling. Brown et al. (2012) and Ekström et al. (2018) emphasize that indicator(s) and/or threshold(s) used to assess system performance under climate stress should be specified with local stakeholders. Risk assessment can then be tailored to meet community/management needs. This approach has already been applied to water management (Brown et al., 2012), flood risk (Steinschneider, McCrary, et al., 2015; Steinschneider, Wi, et al., 2015), cost–benefit analysis (Ghile et al., 2014), and for various hydrologic indices (Singh et al., 2014). The framework can (in theory) also be extended to include additional nonclimatic drivers (e.g., population growth, economic trends) (Brown, 2011).

Although the general principles of the SN approach are now well established (Brown & Wilby, 2012; Chiew, 2006; Prudhomme et al., 2010), there have been a limited number of practical applications in regional- to national-scale management, particularly in data-sparse jurisdictions (Kay, Crooks, Davies, Prudhomme, et al., 2014; Prudhomme, Crooks, et al., 2013). In a relatively data-rich study Prudhomme, Crooks, et al. (2013) demonstrated the framework's utility for flood risk assessment using 154 UK catchments. Catchments were grouped into distinct sensitivity types and used to classify ungauged sites based on their shared physical attributes (Prudhomme, Kay, et al., 2013). Similarly, Köplin et al. (2012) clustered 186

Swiss catchments based on their sensitivity and used results to identify which physiographic features discriminate response type. In an exploratory study Bastola et al. (2012) examined flood sensitivity for four Irish catchments for which the risk of design allowances being exceeded were assessed using the IPCC AR4 climate scenarios. Wilby et al. (2014) applied a similar approach to assess sensitivity of peak flows in the Boyne catchment (Eastern Ireland).

An estimated 0.8 billion people and 50 trillion USD are exposed to a significant (1 in 100 year) river flood event (Scussolini et al., 2016). Given the diversity of hydroclimatological conditions across scales, adopting a national (or regional) allowance for the realization of future climate may fail to address the true emergent risk locally. Hence, critical to avoiding maladaptation is developing tools capable of identifying specific vulnerabilities under uncertain and often data-poor conditions.

The present study develops a coherent framework that can detect those catchment types that carry a high risk of maladaptation. Maladaptation refers to an action that fails to address a viable threat with an appropriate and measured response (Juhola et al., 2016). It reflects a failure to plan without utilizing available facts and applies equally to underadaptation and overadaptation—wherein unnecessary measures may divert resources from higher-risk areas. While it can lead to poor use of resources (e.g., financial, human), badly conceived plans have potentially far-reaching societal, ecological, and environmental consequences and may inadvertently increase risk exposure.

The study focuses on the Republic of Ireland. Herein, a nationally based classification is developed for which catchments are grouped into distinct flood sensitivity types according to their shared physical attributes. Given an expected rise in the frequency and intensity of Atlantic storms, Ireland is particularly vulnerable to increases in fluvial flooding (Matthews et al., 2018). The impact of recent flood events, in combination with a comprehensive flood risk assessment has led to a 10-year €1bn capital program to implement relief schemes (Government of Ireland, 2018; OPW, 2012). As with other jurisdictions, to avoid maladaptation, such infrastructural upgrades will need stress testing against future changes. Here we examine present exposure to climate changes and identify those conditions under which proposed climate change allowances may be inadequate. Thus, while we contribute key information to Irish flood planning and infrastructure standards for a vulnerable sector, in a broader context we outline a framework for risk assessment which has global application. From a hydroclimatological perspective we also identify those processes and land-surface attributes that influence catchment sensitivity—thereby deepening knowledge of flood generating mechanisms. Finally, we advance the SN framework by proposing a method for selecting climate projections that is more equitable with respect to issues of ensemble bias and model interdependence; we also highlight a more robust machine learning technique for regionalization of catchment types.

2. Methods and Data

We apply a SN approach to flood assessment using an initial sample of 35 Irish catchments. Flood responses are evaluated given incremental changes in the annual mean and seasonal distribution of catchment average precipitation. For each increment the precipitation series is altered and input to two different rainfall-runoff models. A weather generator (WGEN) is employed to extend the observed precipitation series and the simulated 20-year flood peak is used to quantify sensitivity to precipitation changes relative to a (1976–2005) baseline. This impact metric is chosen as it represents a standard exceedance threshold used in flood design and can be more reliably estimated given the observed series length (30 years). To account for changes in potential evaporation (PE), a single temperature scenario (+2 °C relative to a baseline) is used. Changes in simulated flood peaks across the sensitivity domain are then used to construct two-dimensional (2-D) response surfaces. To establish a classification, catchments are clustered according to similarities in their response surfaces. Using a random forest (RF) classifier those physical attributes, which are most important in determining group membership, are identified. The model is used to infer the likely sensitivity of an additional 215 sites nationally. These sites are either unmonitored or lack flow data of sufficient quality to undertake robust hydrological model calibration. Exposure to climate risk and the efficacy of design allowances are established using GCM simulations from the Coupled Model Intercomparison Project Phase 5 (CMIP5) ensemble (Taylor et al., 2012). A schematic of the overall analytical framework is given in Figure 1. Details of the key steps are provided in the following paragraphs, followed by an overview of observed data and the CMIP5 ensemble.
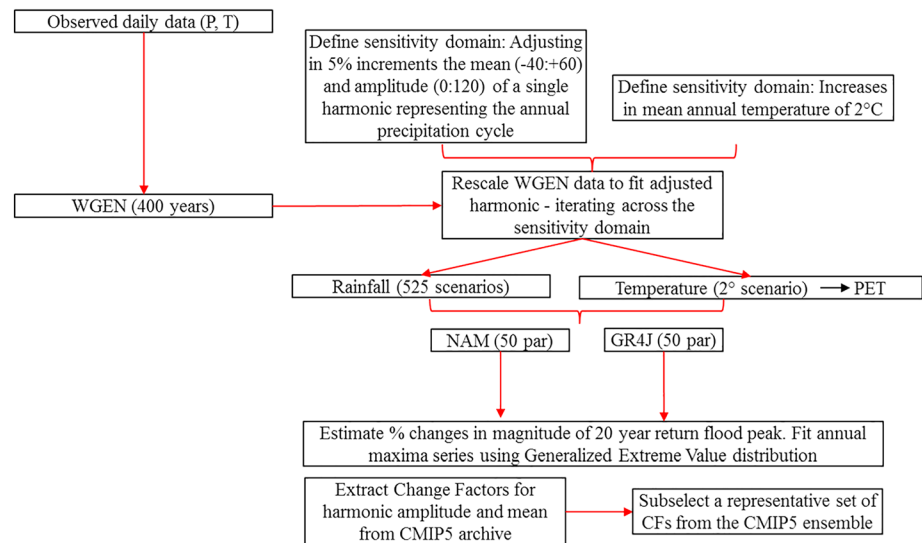
Figure 1. Scenario-neutral methodology used to examine the changing flood response to alterations in precipitation and PET forcing for Irish catchments. WGEN = weather generator; PET=Potential Evapotranspiration.

2.1. Weather Generator

To generate a longer annual maximum series than is available from observed data, response surfaces were developed from climatological series stochastically simulated using a WGEN. Using an extended peak flow series allows greater confidence in the fitted generalized extreme value (GEV) parameters and provides a more robust estimate of flood magnitude. The present study employs the Weather Generator École de Technologie Supérieure (WeaGets) multivariable single-site stochastic WGEN (Chen et al., 2012). The model is fitted (over 14-day periods) to observed precipitation (1976–2005) and temperature in each catchment. Precipitation occurrence is simulated using a third-order Markov chain, while amounts are generated from a two-parameter Gamma distribution. This distribution has been fitted to rainfall amounts across diverse climates for a range of applications (Stephenson et al., 1999; Yang et al., 2005). Additionally, this model configuration is shown to perform well for Irish conditions (Figure S1 in the supporting information). Following the Richardson model, WeaGETS incorporates a smoothing function for the precipitation parameters applied using Fourier harmonics (Richardson, 1981). This reduces the sharp parameter transitions between fitting periods which result from outliers—particularly when using shorter time series. Additionally WeaGETS incorporates an adjustment for the underestimation of low-frequency variability (Chen et al., 2010). Temperature is modeled dependent on precipitation occurrence. Daily precipitation and temperature for a 400-year period are generated. This period length ensures that the key descriptive statistics (monthly mean, variance, percentiles, etc.) of the stochastic series are stationary and match the observations without unduly increasing the computational overheads of using a longer (relative to the 30-year baseline) climate series.

2.2. Rainfall-Runoff Models: Structural and Parameter Uncertainty

To address hydrological model uncertainty, two conceptual rainfall-runoff models were applied. Models differ according to their number of calibration parameters and numeric formulation. Our criteria for selection includes the following: (i) previous application to Irish hydroclimatological conditions; (ii) proven performance for the catchment sample; (iii) computational efficiency; and (iv) representation of alternative model structures (Bastola et al., 2011a, 2011b, 2012; Broderick et al., 2016; Mockler et al., 2016). Based on these criteria, the following two models are selected:

NAM (Madsen, 2000) is a lumped conceptual model, with nine calibration parameters, which simulates the transformation of precipitation to runoff by continuously updating the water content of three coupled stores. Stocks are diminished through evaporative losses and interflow. Overland flow is generated when surface

zone capacity is exceeded; a proportion of this excess is transferred through infiltration to the root zone and groundwater storage. Surface and interflow contributions are routed through two linear reservoirs; baseflow is routed through a single linear reservoir.

GR4J (Perrin et al., 2003) is a lumped model with four calibration parameters. Effective precipitation and soil moisture are estimated from net rainfall. Fluxes from the soil moisture zone along with effective precipitation are partitioned as a fixed 10:90 division between two routing channels. The first channel applies a single-unit hydrograph; the second a unit hydrograph and nonlinear storage function. A gain/loss function is used to simulate groundwater exchanges with deeper aquifers and/or adjoining watersheds.

To ensure transferability between wet and dry conditions, models are calibrated using the first, third, and fifth ranked noncontinuous wettest and driest years, respectively, (Broderick et al., 2016). These years are identified based on catchment average rainfall. For validation the second, fourth, and sixth wettest and driest years, respectively, are used. By simulating the complete time series and examining nonsequential 6-year periods for calibration/validation the internal dynamics and consistency of catchment stores is preserved.

The generalized likelihood uncertainty estimation (GLUE) method is used to investigate flood response across the sensitivity domain (Beven & Binley, 1992). For each rainfall-runoff model 10,000 simulations are conducted for the period 1970–2010 using parameter sets randomly sampled using a Latin Hypercube scheme from uniform distributions (McKay et al., 1979). Following the GLUE procedure, parameter sets are weighted according to calibration performance. Three efficiency criteria are used consisting of the Nash Sutcliffe Efficiency criterion (NSE; equation (2); Nash & Sutcliffe, 1970) applied to the nontransformed (NSE), squared (NSE^2), and square root (NSE$^{0.5}$)-transformed series, respectively. This application ensures consideration of model performance across the hydrograph including those for variability in low (square root) and high (squared) flows. The aggregate efficiency score for each parameter set is estimated as the product of the three individual NSE values. In this respect, each NSE criterion is given an equal weighting. However, by multiplying values parameters must perform well according to each (transformed and nontransformed) to achieve a high overall score. In addition, parameter sets are omitted if they overestimated or underestimated flow volume by more than 15% estimated according to percent bias. This measure does not contribute to the final weighting.

Parameter sets are ranked according to their aggregate efficiency scores. The top 50 performing sets are identified as behavioral and retained. Using simulations from the behavioral parameter sets, the prediction quantiles for each time step are empirically derived according to

$$P\left[\widehat{Z}_t < z\right] = \sum_{i=1}^{\text{NB}} \text{RL}\left[f(\theta_i) | \widehat{Z}_{t,i}, z\right] \tag{1}$$

where P is the selected quantile, θ_i is the ith parameter set, and NB is the number of behavioral parameters. Rescaled Likelihoods (RL) are estimated by scaling the aggregate efficiency scores of the behavioral sets so that they sum to unity. The value of the predicted variable (flow) at time step t by model $f(\theta_i)$ is represented by $\widehat{Z}$. For each model, the 50th percentile is taken as the most likely estimate. It is acknowledged that GLUE necessitates certain assumptions (e.g., use and combination of informal likelihoods, behavioral threshold sample size, and parameter bounds), which, it is argued, affect its statistical validity—particularly in the estimation of prediction intervals (Beven & Binley, 1992; Clark et al., 2011; Mantovan & Todini, 2006; Stedinger et al., 2008). However, as employed here the method is not explicitly intended to provide an estimate of parameter uncertainty in the rainfall response, but rather to provide a robust flow estimate which assumes equifinality in the parameter space (Beven, 2006). Additionally, despite its limitations the method has been applied successfully in numerous environmental and hydrological studies (Beven & Binley, 2014).

2.3. Sensitivity Domain

The present study adopts the sensitivity domain (Kay, Crooks, Davies, Prudhomme, et al., 2014; Kay, Crooks, Davies, & Reynard, 2014; Prudhomme et al., 2010; Prudhomme, Crooks, et al., 2013) used to develop

flood response surface typologies for UK catchments. For this the *y* intercept and amplitude of a single-phase harmonic function representing the baseline annual cycle are fitted to monthly mean values:

$$X_t = X_0 + A \cos\left(\frac{2\pi}{12}(t - \Phi)\right) \tag{2}$$

where X_t is the fitted value for each calendar month, A and Φ represent the amplitude and phase, respectively, and X_0 is the arithmetic mean. In this case, the phase (denoting the month with the greatest mean rainfall) is assumed to be December ($\Phi = 12$). Previous studies highlight the causal effect which changes in these harmonic parameters have on future flood risk (Kay, Crooks, Davies, Prudhomme, et al., 2014; Kay, Crooks, Davies, & Reynard, 2014; Prudhomme et al., 2010; Prudhomme, Crooks, et al., 2013; Prudhomme, Kay, et al., 2013). To traverse the domain, the amplitude and intercept parameters are iteratively adjusted relative to the reference period (1976–2005) by 5% increments. Changes in mean annual precipitation are reflected in alterations to the intercept, which is adjusted between −40% and +60%, while the amplitude, representing changes in seasonality is increased from 0% to 120%, for a total number of 525 combined permutations. These are regarded as plausible given the range of changes suggested by the CMIP5 ensemble and allows for more extreme (possibly as yet unrealized) projections. For each of the 525 perturbations, the annual mean and seasonal amplitude of the stochastically generated 400-year precipitation series is adjusted using multiplicative scaling applied to daily values. To ensure that the annual cycle of the adjusted series matches the perturbed harmonic, scaling is undertaken at a monthly resolution. Hence, with respect to extreme values, changes are reflected in the statistical distribution of daily precipitation, with increases (decreases) in monthly precipitation being reflected in greater (reduced) precipitation intensities. Generated daily temperature values are adjusted using additive scaling. For all 525 climate perturbations, each behavioral rainfall-runoff parameter set is used to simulate the 400-year flow series using the rescaled WGEN series as input. From this the median flow series for each model is calculated according to equation (1) and used to estimate changes in flood magnitude across the sensitivity domain (Figure 1). Two dimensional (2-D) response surfaces are developed for each catchment by plotting the percent change in 20-year flood peak magnitude relative to reference conditions (i.e., zero change) against incremental percent changes in mean annual precipitation amount and seasonality, respectively.

Response surfaces developed for UK catchments show the flood regime to be more sensitive to precipitation than evaporation changes (Prudhomme et al., 2003; Prudhomme, Crooks, et al., 2013; Prudhomme, Kay, et al., 2013). This is also supported by Bastola et al. (2011b), who examined flood sensitivity using the SN framework applied to four Irish catchments. They found that changes in PE associated with temperature increases had a negligible effect on flood magnitude. Thus, our assessment is restricted to a single scenario representing an absolute increase in mean annual temperature of 2 °C relative to 1976–2005.

2.4. Flood Frequency Analysis

The magnitude of the 20-year return period flow event is estimated using the GEV distribution fitted to the 400-year simulated annual maximum series. This is estimated from the median flow series derived according to the GLUE procedure using the identified behavioral parameter sets (Ahilan et al., 2012; Cameron et al., 1999). The cumulative distribution function of the GEV distribution is inverted and evaluated for the 20-year return period/percentile (rp) according to

$$F^{-1}(rp) = \zeta \frac{\beta}{\kappa}\{-\ln[(rp)]^{-\gamma} - 1\} \tag{3}$$

where ζ, β, and γ represent the location, shape, and scale parameters of the GEV distribution, respectively. Parameters are estimated using the method of maximum likelihood.

2.5. Clustering

To identify catchments with similar responses, the 2-D surfaces for each rainfall-runoff model and catchment are first converted to a single vector and horizontally concatenated. All vectors are arranged into a matrix of size 35 × 1,050—representing the number of observations (catchments) and variables (points on the response surface), respectively—and input to a *k*-means clustering procedure (Lloyd, 1982). Accordingly, the algorithm partitions the input matrix into *k* clusters for which each catchment response

surface is assigned to the cluster with the nearest centroid based on Euclidean distance. The centroid is estimated as the arithmetic mean of assigned cluster members. As clusters are influenced by the initial position, 100 random initialization points are used. That seed point which minimizes the cost function is retained. The error function used is expressed as

$$J = \sum_{j=1}^{k} \sum_{i=1}^{n} \left\| x_i^{(j)} - c_j \right\| \tag{4}$$

where k and n represent the number of clusters and observations, respectively; $x_i^{(j)}$ denotes the ith member of the jth cluster, the centroid of which is given by c_j. This algorithm is used in conjunction with the Calinski-Harabasz (CH) efficiency criterion (Calinski & Harabasz, 1974) to optimize the number of clusters. The criterion seeks a value for k, which simultaneously minimizes/maximizes the within/between cluster variance:

$$CH = \frac{B_k}{W_k} \times \frac{N-k}{k-1} \tag{5}$$

where N represents the number of data points. W_k and B_k denote the within and between cluster sum of squares, respectively, calculated using the squared Euclidean distance. Convergence to a local optimum is achieved when group membership is stable over successive iterations. An individual 2-D centroid response surface is derived for each model and cluster. This is calculated as the arithmetic mean of the individual (1,050) grid points averaged across cluster members. This vector is split according to each model and reshaped into the original response surface dimensions (21×25).

2.6. Response Surface Characteristics

Differences in sensitivity between the response surface centroids for each cluster are quantified based on the mean rate of change (gradient) along the x (horizontal) and y (vertical) axes, respectively. This demonstrates the degree of sensitivity to unit changes in each harmonic parameter independently, without explicitly considering interactive effects. It is calculated based on the maximum difference in the percent flood peak response between each neighboring vector element or grid point on the 5% interval along the x and y axes, respectively.

Also calculated is the maximum slope for each centroid. Here slope is estimated as the change in magnitude per unit distance along the path of steepest ascent/descent from a grid point to one of its eight nearest neighbors according to (O'Callaghan & David, 1984):

$$S_{D8} = \max_{gp=1,8} \frac{v_9 - v_{gp}}{h \varnothing(gp)} \tag{6}$$

where $\varnothing(gp) = 1$ for $gp = 2, 4, 6$, and 8 (E, S, N, and W neighbors) and $\varnothing(gp) = \sqrt{2}$ for $gp = 1, 2, 5$, and 7 (NE, NW, SW, and SE neighbors). This measures the rate of change across the surface in the x and y directions simultaneously and is indicative of overall sensitivity.

2.7. Random Forest Classifier

Classification Trees (CTs) are predictive models which use a set of decision rules inferred from features (predictor) of the input data to determine group membership of the predictand. The model constitutes a hierarchical tree with root, decision, and leaf nodes. While having powerful analytical capabilities, it is recognized that CTs are prone to overfitting (Hastie et al., 2009). By aggregating predictions from an ensemble of CTs, wherein the influence of individual biases are offset by other ensemble members (EMs), a RF can generalize more successfully (Breiman, 1996, 2001). RFs are suitable for mixed data types and can handle collinear/interactive predictors. The ensemble is composed of multiple CTs, each developed using a bootstrapped sample of the original data. In addition, at each decision node a random subset of predictors is selected from which the most important split features are retained. This reduces correlation between individual trees and lessens the influence of noise/outliers. While the RF does not produce an explicit model revealing the decision process and relationship between predictors (as in the cases of CTs) it does return a measure of predictor importance.

Here a RF is developed using the physical attributes (physical catchment descriptors; PCDs) of the catchment sample as predictors. Catchment type, identified using the *k*-means procedure applied to the response surfaces, is used as the (categorical) predictand. Based on its contribution to model accuracy the relative importance of each PCD in differentiating catchment types is examined. Features are interpreted to determine which processes and land-surface attributes influence sensitivity. The RF is also employed to predict the sensitivity class of ungauged or data-sparse catchments (Booker & Woods, 2014; Snelder et al., 2013). The RF used constitutes 10,000 CTs, each grown using a subset (80%; with replacement) of cases. The remaining "out-of-bag" (OOB) cases (20%) are retained to independently estimate predictor importance and ensemble error. The RF algorithm thus facilitates a type of cross validation which is robust in cases where the number of observations is limited. At each decision node the algorithm selects the best split from a random subset (15) of all available (19) predictors according to Gini's diversity index. The OOB error is calculated as the proportion of cases which are misclassified (*MR*), estimated as

$$MR \approx MR^{\mathrm{OOB}} = c^{-1} \sum_{i=1}^{c} I\left(\widehat{Y}(J_i) \neq Y_i\right) \qquad (7)$$

Where $I(\cdot)$ denotes the indicator function, Y the observed class labels, and c is the number of cases. Finally, $\widehat{Y}$ represents the OOB prediction and J the vector of descriptors. Each tree is grown to a maximum depth thus avoiding uncertainty issues related to predictor selection and pruning method. During model training the RF algorithm identifies the most important predictors. Importance is quantified by observing the effect that randomly permuting each predictor has on the OOB error. A standardized measure of importance is returned—estimated as the average difference in prediction error across the ensemble divided by the standard deviation. Ensemble predictions are made by aggregating the classification predicted by EMs. For a given case that class with the majority vote is considered the most likely. To investigate uncertainty, the RF algorithm also returns the probability of the predicted class. For each CT the posterior probability at a particular node is the number of cases assigned to that node, which have the same observed class, divided by the total number of cases assigned to that node. The posterior probabilities returned by individual CTs are averaged across the ensemble.

2.8. Catchment Selection and Observed Data

Catchments were selected on the basis that they (i) have good quality, long-term observational data; (ii) are minimally impacted by human activity; (iii) constitute a representative sample of different catchment types; and (iv) have associated PCDs. In all, 35 catchments (Murphy et al., 2013; Figure 2) meet these criteria with flow data that variously cover the years 1973–2001. Daily flow series were obtained from the Office of Public Works (OPW; http://waterlevel.ie/) and Environmental Protection Agency (http://www.epa.ie/hydronet/). The physical attributes of each catchment are obtained from the OPW's Flood Studies Update (FSU; http://opw.hydronet.com; Mills et al., 2014). PCDs provide information about the climatological, soil and morphometric properties of each catchment (see Tables 1, S1, and S2). Relative to a larger sample, the catchments used are representative of hydroclimatological conditions across the island, but with a recognized underinclusion of smaller upland catchments located along coastal margins. Urban extent is low overall. For the 215 catchment sample the majority (~95%) have <6% urban extent, with only seven having coverage >6%. The greatest urban coverage by a considerable margin (68%) is for the river Slang (ID: 9011). To calibrate hydrological models we use gridded (1 × 1 km) daily precipitation and temperature data (Walsh, 2012) area averaged to provide a single representative baseline for each catchment. Daily potential evapotranspiration is estimated from air temperature and radiation following the method of Oudin et al. (2005). This is favored over less parsimonious but more physically based methods (e.g., Penman-Monteith), which have greater data requirements (e.g., wind speed, humidity) not available for all study catchments (Kay et al., 2013).

2.9. CMIP5 Ensemble

CMIP5 simulations of monthly precipitation covering the period 1850–2100 and relating to one of four different Representative Concentration Pathways (RCP2.6, RCP4.5, RCP6, and RCP8.5) are used to examine the flood risk exposure of individual catchments (Table S3). For each EM and all 215 catchments, Change Factors (CFs; Anandhi et al., 2011; Diaz-Nieto & Wilby, 2005) are calculated based on the percent difference in mean monthly precipitation between the 1976–2005 baseline and three separate 30-year horizons (2010–
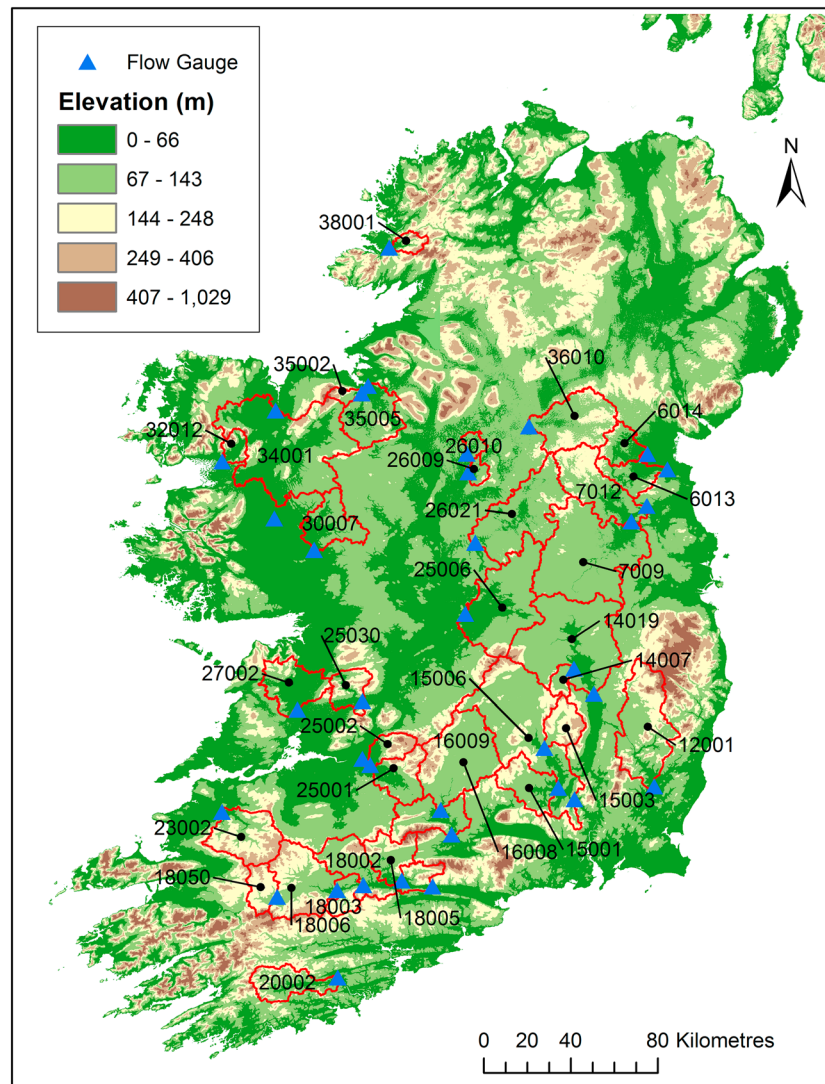
Figure 2. The location, boundaries, and identification number of the catchment sample.

2039; 2040–2069; 2070–2099). Precipitation series are extracted for the GCM grid point directly overlying each catchment centroid. Following Prudhomme et al. (2010), CFs are calculated by differencing all continuous 20-year blocks within the 30-year window. This reduces potential sampling uncertainty introduced by relying on a single (30-year) value of baseline and future climate (Kendon et al., 2008; Räisänen & Ruokolainen, 2006). To estimate changes in amplitude and mean annual precipitation, a harmonic function (equation (2)) is fitted to the median of the block-sampled CFs. This is applied to each 30-year horizon, EM and 215 catchments. Extracting changes in parameters of the sensitivity domain allows the CMIP5 projections to be overlain on the 2-D response surfaces, from which the corresponding change in flood magnitude can be derived. Also estimated from the CMIP5 ensemble are absolute changes in mean annual temperature for the same RCPs and time horizons.

2.10. CMIP5: Ensemble Member Subselection

Their computational cost mean experiments like CMIP5 rely on autonomous modeling groups. However, groups differ with respect to the number of simulations they contribute, the specific model(s) used, and which uncertainty component(s) they consider (e.g., parameter perturbation, initial conditions, structural differences, and emission scenario). Moreover, GCMs developed by different groups can share a similar formulation and hence many of the same assumptions/errors—an issue also affecting successive model

Table 1
Physical Catchment Descriptors (PCDs) Derived for the Flood Studies Update (FSU; Mills et al., 2014)

PCD abbreviation	Descriptors explained	Minimum (215)	Maximum (215)	Minimum (35)	Maximum (35)
ALLUV (Prop)	Proportional extent of floodplain alluvial deposit	0.00	0.11	0.01	0.10
AREA (km^2)	Catchment area (km^2)	5.46	7980.41	88.82	2460.27
ARTDRAIN (Prop)	Proportion of catchment area mapped as benefitting from arterial drainage schemes	0.00	0.37	0.00	0.28
ARTDRAIN2 (Prop)	Proportion of river network length included in Arterial Drainage Schemes	0.00	0.85	0.00	0.78
BFIsoil (index)	Soil baseflow index (estimate of BFI derived from soils, geology and climate data)	0.26	0.91	0.28	0.83
DRAIND (km/km^2)	Drainage density (km/km^2)	0.04	2.64	0.54	2.37
FAI (Prop)	Flood Attenuation Index	0.01	0.52	0.06	0.27
FARL (index)	Flood attenuation by reservoirs and lakes	0.63	1.00	0.81	1.00
FLATWET (index)	PCD summarizing proportion of time soils expected to be typically quite wet	0.54	0.73	0.54	0.73
FOREST (Prop)	Proportional extent of forest cover	0.00	0.56	0.24	0.35
MSL (km)	Mainstream length (km)	2.84	214.61	17.47	129.08
NETLEN (km)	Total length of river network above gauge (km)	2.94	6428.92	64.67	2669.46
PEAT (Prop)	Proportional extent of catchment area classified as peat bog	0.00	0.80	0.00	0.53
S1085 (m/km)	Slope of main stream excluding the bottom 10% and top 15% of its length (m/km)	0.10	31.16	0.20	13.26
SAAPE (mm)	Standard period average annual potential evapotranspiration (mm)	448.28	562.64	459.60	532.60
SAAR (mm)	Standard period average annual rainfall (mm)	710.76	2464.73	814.07	1784.36
STMFRQ (no.)	Number of segments in river network above gauge	1	5490	35	3523
TAYSLO	Taylor-Schwartz measure of mainstream slope (m/km)	0.11	8.32	0.13	1.05
URBEXT	Index of Urban Extent (% coverage)	0	68.1	0	2.1

Note: Also shown is the range in values for 215 catchments included in the FSU and values for the 35 catchments used in this study. BFI = baseflow index.

generations (Knutti et al., 2013; Masson & Knutti, 2011). Here biased sampling leads to a disproportionate weighting of the respective model sensitivities, resulting in a skewed interpretation of likely changes. Providing statistically robust descriptors of future climate is conditional on the independence of EMs (Déqué & Somot, 2010; Greene et al., 2006; Masson & Knutti, 2011; Mendlik & Gobiet, 2016), with several studies highlighting the effect which redundancies have on the effective ensemble size (Cannon, 2015; Pennell & Reichler, 2011; Pirtle et al., 2010).

Dependent on horizon and RCP up to 22% (#10) of CMIP5 EMs are produced by the same GCM (CSIRO-Mk3–6-0). To address possible redundancies, the partitioning around medoids procedure (Kaufman & Rousseeuw, 2005) is used to identify a representative ensemble subset (herein referred to as CMIP5_sub). The *k*-medoid algorithm differs from *k*-means in that the point used to quantify within/between cluster differences is not the centroid but a member of the subset (medoid). As the objective is to identify that EM which is most representative of a given subspace, this constitutes a more appropriate approach. Subselection is conducted using the GCM grid box precipitation scenarios for each (215) catchment, 30-year horizon, and RCP, respectively. To correspond with the sensitivity domain, EMs are clustered according to similarity in their intercept and amplitude. Parameters are standardized (*z* score) prior to clustering and similarity is measured in squared Euclidean distance. It is highlighted that clustering algorithms are biased toward regions of higher density, which has implications for excluding EMs located at the extremities - potentially underestimating risk (Cannon, 2015). To address this, the KKZ (Katsavounidis-Kuo-Zhang) initialization procedure is used to identify seed points which maximize ensemble diversity (Katsavounidis et al., 1994). In addition, the number of clusters is selected as the minimum required for the subset to span the original ensemble range.

2.11. Harmonic Function: Phase Assumption

In this study a single-phase harmonic (equation (2)) is used to (i) scale the WGEN series so as to traverse the sensitivity domain according to changes in the precipitation cycle, (ii) to estimate percent changes in the amplitude and mean of individual CMIP5 projections. As visual presentation of response surfaces is limited to two dimensions, the phase is held constant and set to December. This represents the median month for which the annual precipitation cycle peaks across the catchment sample. The assumption of a December phase is also commensurate with the CMIP5 ensemble, for which the majority (65% considering all 215

catchments, RCPs, and time horizons) of model runs indicate a more pronounced winter peak. This signal generally strengthens through each consecutive time horizon and is most distinct for 2070–2099 under RCP8.5, wherein 95% of EMs indicate a winter phase. Kay, Crooks, and Reynard (2014) explored the influence which a fixed phase may have on flood response across the sensitivity domain for nine typical response types found in the United Kingdom. Results show that this assumption is more/less impactful depending on the catchment and climate ensemble considered. In some cases catchments revealed increased sensitivity to alternative phases. However, the authors highlight that this simplification is supported by the majority of climate projections indicating a winter phase.

3. Results

3.1. Rainfall-Runoff Model Development

Figure 3 illustrates hydrological model performance in reproducing a series of hydrological indices estimated using the period for which all observed flow data are available; also shown are the NSE validation scores. In both cases model performance is examined using the median GLUE simulation. Given the domain used for sensitivity testing, indices relating to catchment memory (autocorrelation) and interseasonal variability (seasonal elasticity: i.e., link between summer/winter rainfall and winter/summer flow response); (Visessri & McIntyre, 2016) as well as peak flows (high pulse count) are employed (Hrachowitz et al., 2014; McMillan et al., 2017; Westerberg et al., 2016). Differences between models, as well as validation periods, are most evident for NSE^2. The highest validation scores (0.96; $NSE^{0.5}$) are returned for the river Glyde (ID: 6014) by GR4J. In contrast, NAM returns the lowest score (0.64; NSE^2) for the river Bandon (ID: 20002). Generally, GR4J performs better than NAM for the majority of catchments, particularly those with a lower baseflow index (BFI), which is indicative of runoff—as opposed to groundwater—dominated systems. In addition, both models reproduce variations in the hydrological signatures between catchments. Each captures the runoff coefficient, BFI, annual runoff, and coefficient of variation. However, for catchments with a low BFI, models tend to underestimate the high flow variability and pulse count. Moreover, both consistently underestimate the autocorrelation coefficient of the observed mean monthly series for lags of 1, 3, and 6 months.

3.2. CMIP Projected Climate Changes

Changes in the harmonic mean and amplitude of the annual precipitation regime projected by CMIP5_Sub and CMIP5 for the combined 215 catchments are shown in Figures 4 and S2, respectively. Mean annual precipitation totals are expected to increase marginally (<10% based on the ensemble median). However, this conceals marked changes in the seasonal distribution: projections generally suggest an increase in the amplitude of the annual regime consistent with a narrative of wetter winters and drier summers. This trend is most pronounced for 2070–2099 under RCP8.5. Figure 4 illustrates the level of uncertainty associated with precipitation wherein changes in the harmonic mean span a sign change irrespective of the time period and RCP considered. By the end of the 21st century mean annual precipitation is projected to decrease/increase by up to ~25% relative to baseline conditions. Changes in seasonality are equally uncertain. However, the signal does notably strengthen over progressive horizons for the high emissions RCP6 and RCP8.5 scenarios. Figure S2 shows changes in mean annual temperature projected for the 215 catchments by CMIP5 for each horizon and RCP scenario. This confirms that the majority of EMs are within the +2 °C scenario (relative to 1976–2005) used for sensitivity testing (Figure S2).

Figure 4 presents results of the ensemble subselection process for a single catchment. Herein, the selected members are shown to capture regions of high density and span the original ensemble space. Dependent on the RCP, catchment, and time horizon clustering leads to a reduction in ensemble size of between 0% and 87%, with a median reduction of 56% across all permutations (i.e., RCPs, 30-year horizons and 215 catchments). Over successive horizons and RCPs there is a similar variation in the proportion of projections retained. However, considering only those models which contribute multiple runs (>1), up to 41% of EMs are assigned to a cluster containing a simulation from the same GCM. This varies dependent on the horizon and RCP, with greater redundancies for 2070–2099 and RCP8.5, reflecting the lesser significance of natural variability and the more pronounced effect of individual climate model sensitivities.
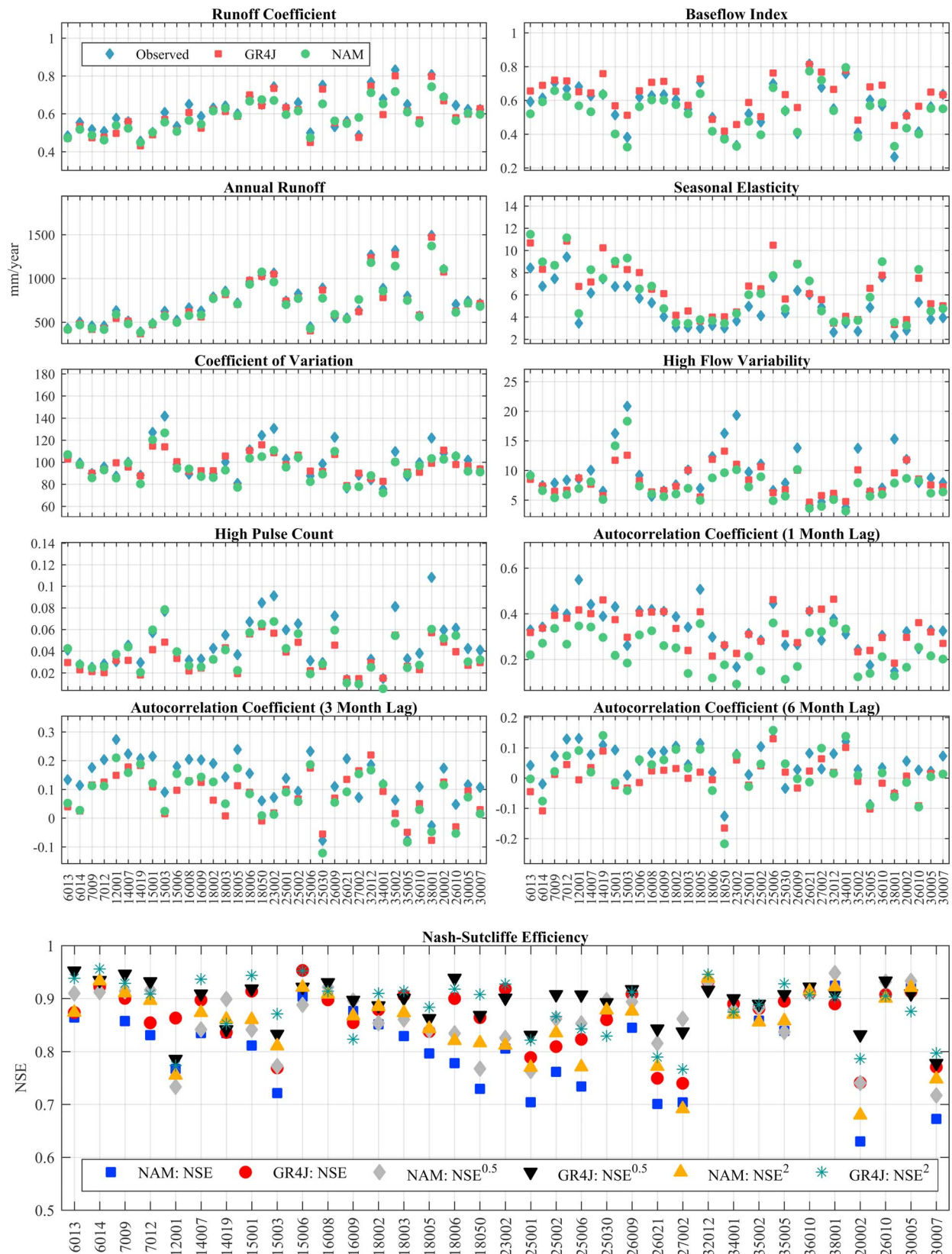
Figure 3. Observed and rainfall-runoff model (GR4J and NAM) simulated hydrological signatures estimated for each catchment using the period for which observed flow data are available. Also shown (lower panel) are the Nash Sutcliffe Efficiency (NSE) validation scores for each catchment and rainfall-runoff model.
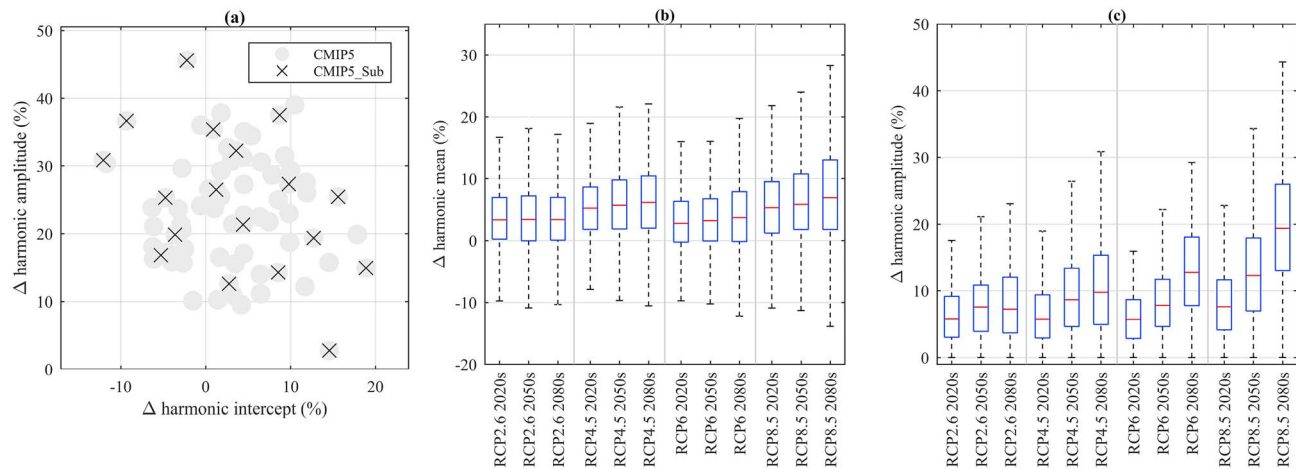
Figure 4. Ensemble members (*k*-medoids) for the Boyne (ID: 7012; 2070–2099; RCP 8.5) subselected using the partitioning around medoids algorithm (a). Also shown are percent changes in the mean annual amount (harmonic mean; b) and seasonality (harmonic amplitude; c) of the precipitation cycle described using a single-phase harmonic function (equation (2)). Changes are examined for three future time horizons relative to the 1976–2005 baseline and for four different RCP scenarios and three future time horizons: 2010–2036 (2020s), 2040–2069 (2050s), and 2070–2099 (2080s). Plots are developed using the subselected Global Climate Model simulations (CMIP5_Sub) from the CMIP5 archive stored at a monthly resolution for all 215 catchments (Table S3). Boxplots show the median (central mark; q2) along with the 25th (bottom; q1) and 75th (top edges; q3) percentiles. Whiskers extend to q2 ± 1.57(q3 − q1)/sqrt (ens), where ens is the number of ensemble members. RCP = Representative Concentration Pathways; CMIP5 = Coupled Model Intercomparison Project Phase 5.

Given the complexity of the global climate system establishing the credibility of GCMs—considering the multitude of variables, physical processes, metrics, and spatiotemporal scales involved (Harrison et al., 2015; Perez et al., 2014; Vaze et al., 2011)—is beyond the present study's scope; however, the performance of each EM in reproducing the parameters of a single-phase harmonic (equation (2)) fitted to the annual cycle of precipitation and temperature for the 215 study catchments is provided in Figures S3 and S4, respectively.

3.3. A Catchment Typology of Flood Sensitivity
3.3.1. Individual Catchments

Figures 5 and 6 display 2-D response surfaces developed for 35 catchments using the median simulation from NAM and GR4J, respectively. Overlain on each plot are percent changes in the harmonic mean and amplitude of the precipitation regime projected for 2070–2099 for each RCP by individual CMIP5_Sub EMs. Also shown are indicative (10%, 20%, and 30%) climate change allowances which would provide additional capacity in the design of new flood infrastructure to accommodate future climate change (OPW, 2015). Response surfaces relating to the earlier 30-year horizons are given in Figures S5–S8. Generally, peaks are shown to increase incrementally in line with iterative growth in the applied precipitation mean and amplitude, respectively. This reflects their singular and interactive effects on the catchment water balance and flood processes. Sensitivity to each parameter independently is expressed as their maximum gradient along each axis (Table S2). The maximum RS slope (S_{D8}) is indicative of interactive effects (equation (6)).

Differences in the magnitude and shape of the response pattern reflect the extent to which catchments dampen or amplify seasonal/annual scale precipitation changes. It also highlights the role played by local rainfall-runoff processes in determining the hydrological response and ultimately flood generation across the sensitivity domain. All catchments are more sensitive to changes in mean amounts as opposed to seasonality; however, relative to one another, some are more responsive to increases in seasonal amplitude—indicated by their greater rate of change along the *x* axis (Blackwater; ID: 18002; GR4J; maximum *x* axis gradient: 0.41). Alternatively, as in the case of the river Barrow (ID: 14019; GR4J; maximum *y* axis gradient: 2.53), some catchments are relatively more sensitive to changes in mean annual receipts, as is shown by their gradient along the *y* axis. The influence which interactive effects have is illustrated by the response surface for the river Slaney (ID: 12001), which is relatively sensitive to changes along both axis and has a high maximum S_{D8} value (67.3°; GR4J).
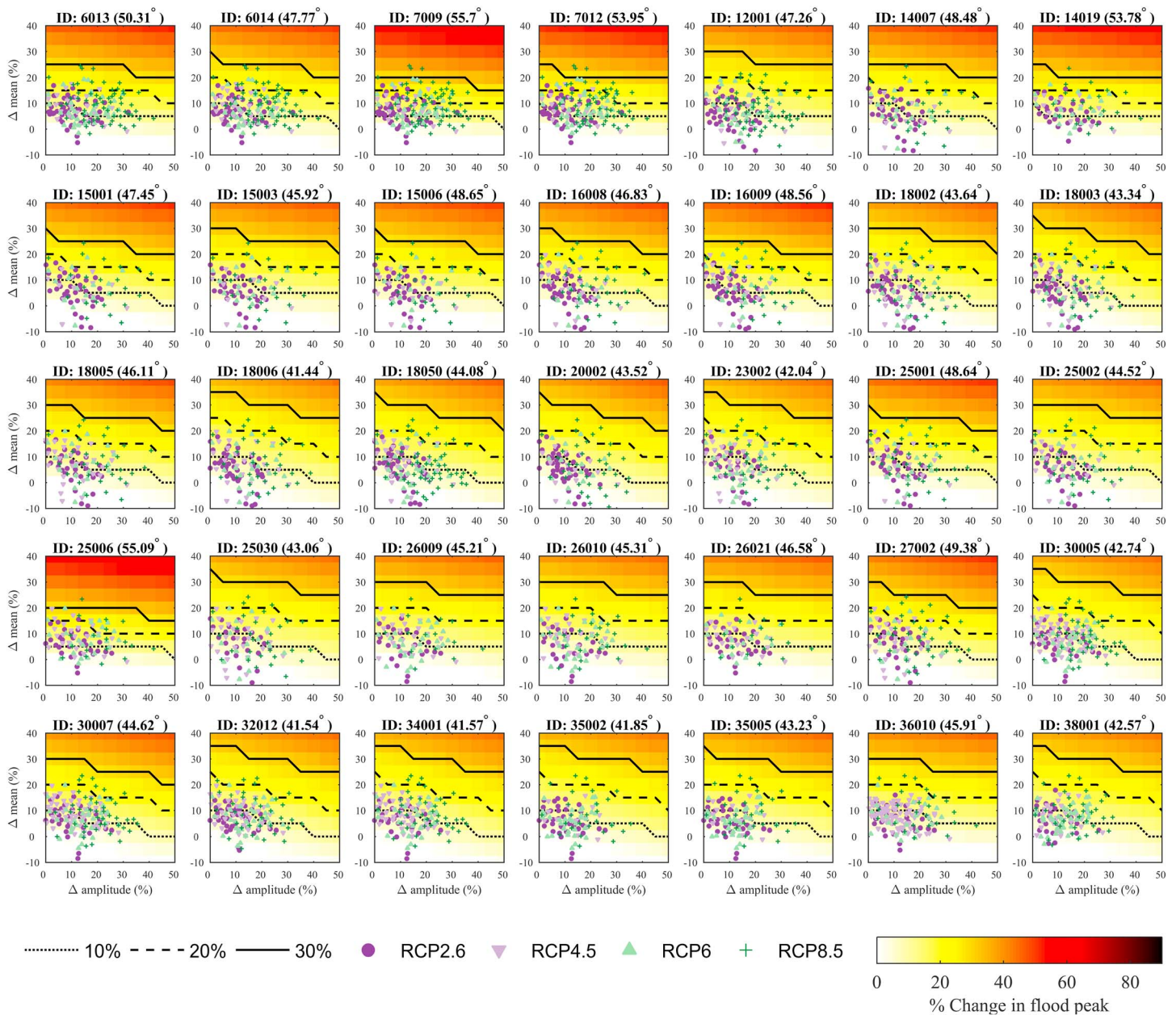
Figure 5. Changes (%) in the magnitude of a 20-year return period flood event for incremental changes (5%) in harmonic parameters representing the mean amount (−10% to +40%; *x* axis) and seasonality (0% to 50%; *y* axis) of the annual precipitation cycle. Surfaces are developed for each of the 35 catchments using the median Generalized Likelihood Uncertainty Estimation simulation from the NAM model. Overlain on each plot are changes (%) in the harmonic mean and amplitude projected for the 2070–2099 relative to 1976–2005 under RCP8.5 by each member of the CMIP5_sub ensemble. For plotting the range is constrained between 0% and 90%. Also shown is the 10%, 20%, and 30% climate change allowance. Lines are interpolated using the technique of nearest neighbor. Also given in brackets is the maximum slope (S_{D8}) of the surface calculated according to equation (6). RCP = Representative Concentration Pathways; CMIP5 = Coupled Model Intercomparison Project Phase 5.

When combined with the CMIP5_Sub simulations, the response surfaces (Figures 5 and 6) highlight the contrasting sensitivity of individual catchments to precipitation changes. Most cases reveal that a 10% climate change allowance would be insufficient to counter projected flooding. Conversely, a 20% allowance would be sufficient to cover the majority of CMIP5_Sub projections across catchments. For example, most simulations for the river Owenbeg (ID: 35002) are within the 20% boundary. However, this is not the case for all catchments—as demonstrated by the Boyne (ID: 7009; Figure 6) which has a large proportion of GCM projections lying beyond the frontier of this allowance.
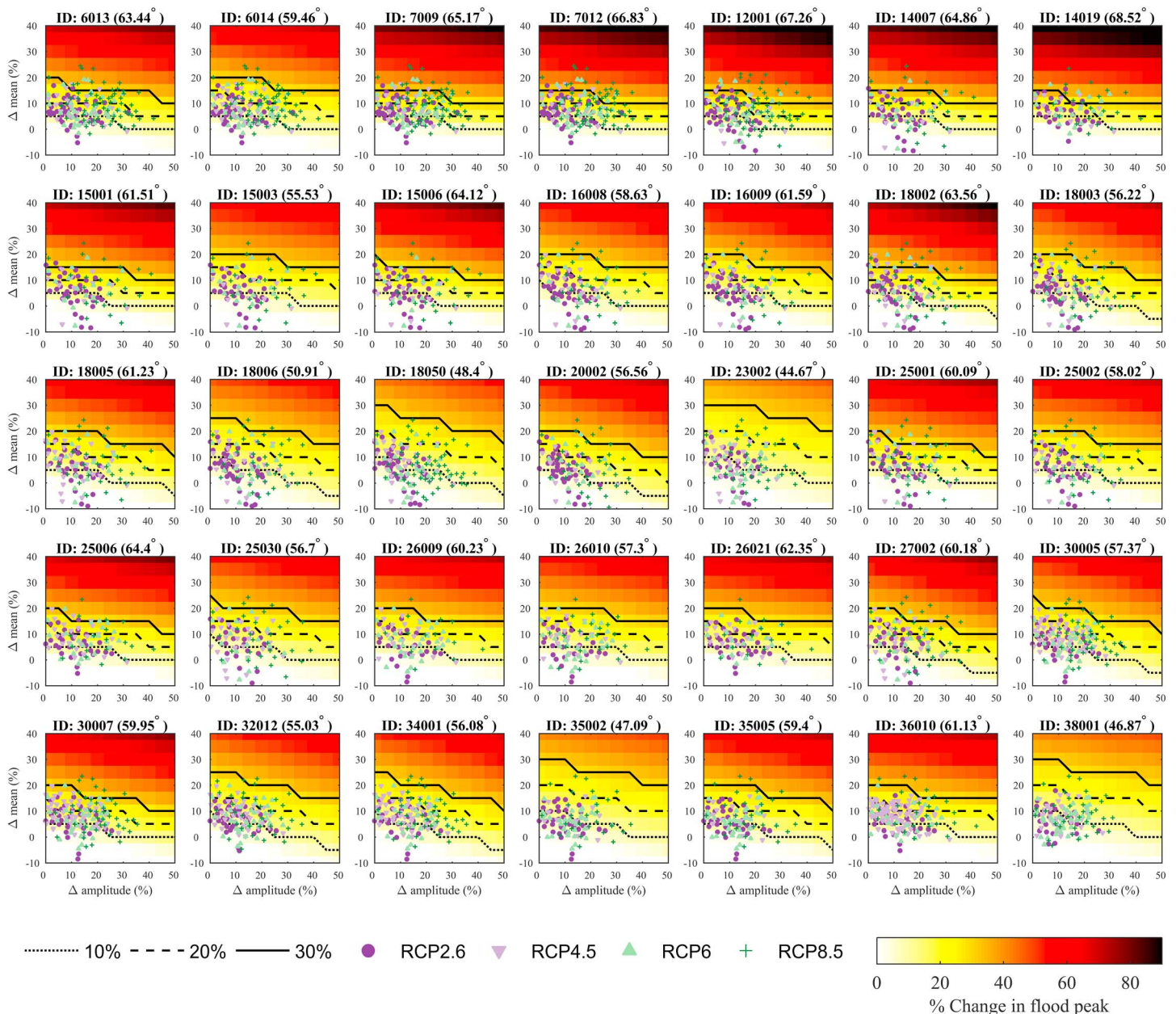
Figure 6. As in Figure 5 but for GR4J.

Figures 5 and 6 also show the extent to which rainfall-runoff model structural uncertainty have on the response surfaces. In most cases, both GR4J and NAM produce surfaces with a similar pattern. However, simulated changes in the flood peak magnitude under the same forcing scenario differ noticeably. Typically, GR4J is shown to have a more sensitive peak response than NAM. In the case of both models a 30% allowance (based on the period 2070–2099 and RCP8.5) would be sufficient to cover between 80 and 100% of CMIP5_Sub projections, with the Boyne (ID: 7012) remaining most exposed.

3.3.2. Response Surface Typologies

Response surfaces developed using the median simulation from both models for each of the 35 sample catchments were classified using a k-means clustering algorithm. Based on (dis)similarities in their surfaces the CH evaluation criterion returns five clusters with membership ranging between 4 and 12 catchments (Table 2). Figure 7 shows each cluster centroid, the maximum surface slope (S_{D8}; equation (6)), and the location of catchment members. Centroids represent the arithmetic mean of the response surfaces assigned to

Table 2
Mean Gradient (y and x Axes, Respectively) and Mean Slope (S_{D8}) of the +2 °C Centroid Response Surface for Each Rainfall-Runoff Model

Cluster	Catchment members	Harmonic mean (*y* axis) GR4J	Harmonic mean (*y* axis) NAM	Harmonic amplitude (*x* axis) GR4J	Harmonic amplitude (*x* axis) NAM	Mean slope (°) GR4J	Mean slope (°) NAM
(a)	7009, 7012, 12001, 14007, 14019	2.05	1.23	0.22	0.14	64.0	51.1
(b)	6013, 15001, 15006, 18002, 25001, 25006, 30007	1.69	1.09	0.26	0.17	59.6	47.7
(c)	6014, 15003, 16008, 16009, 18005, 25002, 25030, 26009, 26010, 26021, 35005, 36010	1.44	0.98	0.24	0.16	55.4	44.9
(d)	18003, 18006, 20002, 27002, 30005, 32012, 34001	1.29	0.88	0.33	0.22	53.1	42.2
(e)	18050, 23002, 35002, 38001	0.97	0.85	0.23	0.21	44.9	41.2

Note. Also listed is the ID number of catchments assigned to each cluster.

each cluster. Differences between centroids with respect to gradient along the *x* (horizontal) and *y* (vertical) axis, respectively, are given, also listed is their mean slope (S_{D8}). By considering changes along the *x* and *y* axes simultaneously, S_{D8} provides a measure of the overall sensitivity. Hence, centroids are arranged (Figures 7a–7e) from most to least sensitive according to this metric.

Cluster (a) is most sensitive to changes in the harmonic mean. In contrast, the greatest proportional increases in flood magnitude associated with changes in seasonal amplitude are returned by clusters (d) and (e), with the degree of differentiation between each, dependent on rainfall-runoff model used. GR4J shows a clearer distinction between clusters. Cluster (a) is noted as being the least sensitive to changes in the seasonal distribution.

As shown in Figure 7 there is a spatial aspect to the distribution of cluster members, reflected by an east-west gradient. Generally, catchments from cluster (a) are situated on the east coast and encompass the Boyne (ID:
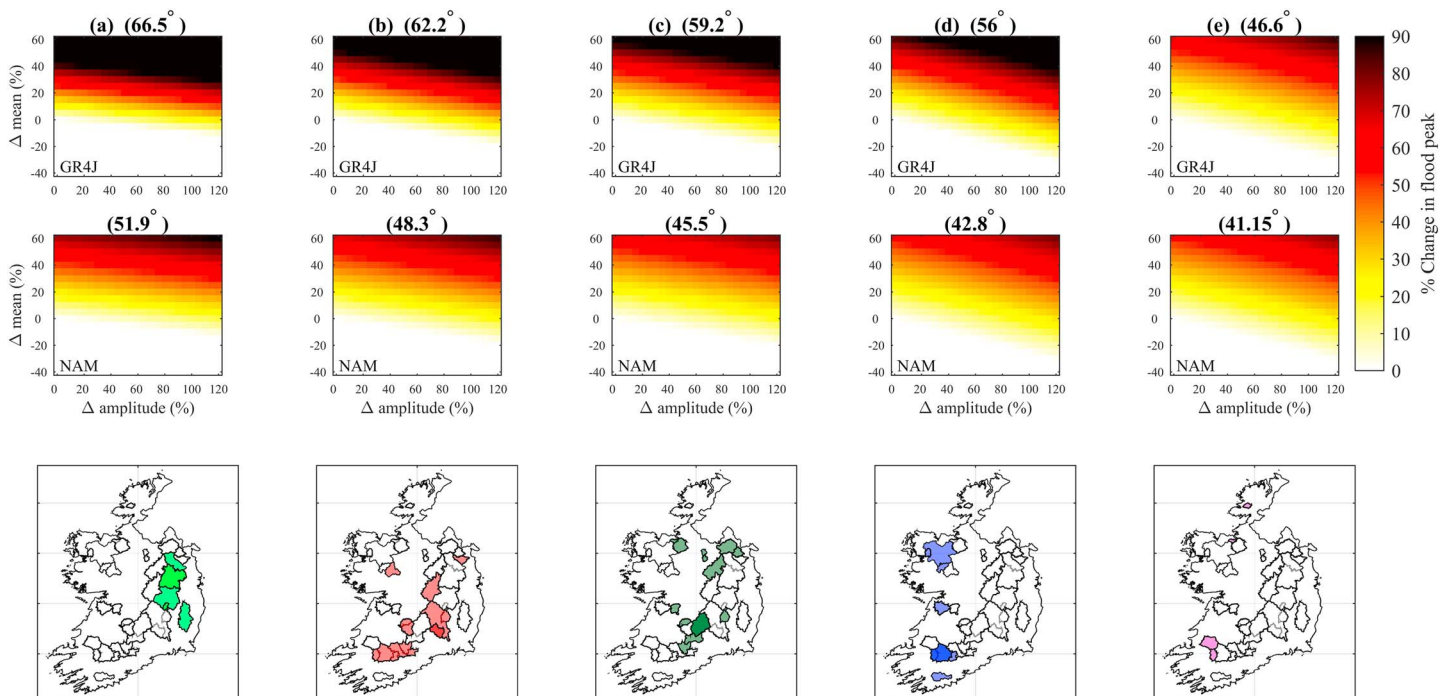

Figure 7. The centroid of five clusters for each rainfall-runoff model (GR4J and NAM) showing the centroid response surface relating to a 2 °C temperature increase. Centroids are derived as the arithmetic average of the grid points from the response surfaces of each cluster member and hydrological model. Response surfaces show change (%) in the magnitude of a 20-year return flood event for corresponding changes (%) in the mean amount (−40% to +60%; *x* axis) and seasonality (0% to 120%; *y* axis) of the annual precipitation cycle. Clusters are arranged (a–e) based on the mean slope (equation (6)) of their centroid. For plotting the range is constrained between 0% and 90%. Also given in brackets is the maximum slope (S_{D8}) of the surface calculated according to equation (6). The lower row shows the location of each cluster member.

7009, 7012), Slaney (12001), and Barrow (ID: 14007, 14019). Catchments from clusters (b) and (c) are located in the Midlands (ID: 26021, 25006, and 26009), [ID: Inny (26021), Brosna (25006), and Rinn (26009)], as well as in the south/southeast [Nore (ID: 15003, 15006), Suir (ID: 16008, 16009)], northwest [Mulkear (ID: 25001, 25002), Owenmore (ID: 35002, 35005), Erne (ID: 36010)] and northeast [Glyde and Dee (ID: 3016, 6014)]. Members of cluster (d) are found further west (ID: 34001) and in the south (ID: 18002 to 18006 and 20002). Members of cluster (d) are found further west (Moy and adjoining catchments (ID: 34001)) and in the south (Blackwater subcatchments (ID: 18002–18006) and Bandon (ID: 20002)). Finally, catchments [Feale (ID: 23002), Owenmore (ID: 35002, 35005), and Owenea (ID: 38001)] from group (e) are situated along the furthermost south/north-western margins of the catchment sample.

3.3.3. Typology of Catchments

Several hydrological features help to differentiate between sensitivity types. Generally, by altering the dynamics of longer-term storage and release, changes in the mean and amplitude of precipitation are likely to influence regime change to a greater degree in catchments which have a longer 'memory' (i.e., predominantly lowland type systems with permeable geology and greater storage capacity). In contrast, as they have less storage capacity, catchments with a shorter memory (i.e., upland systems with impermeable geology and thin peaty soils) are less sensitive to the effects of interannual and interseasonal precipitation changes. The influence of memory is also reported by Prudhomme, Crooks, et al. (2013), Prudhomme, Kay, et al. (2013) for the UK where catchments with greater storage potential were also found to be more sensitive to the types of interseasonal changes in precipitation investigated.

For Ireland, catchments from cluster (a) are classified as being the most sensitive (Table 2). However, these catchments are generally less responsive to increases in precipitation amplitude as opposed to the harmonic mean. This indicates that, due to decreases in summer precipitation, these catchments are better able to offset—through greater available storage and/or more favorable antecedent conditions (such as lower soil moisture) – corresponding increases in winter associated with an amplified regime. Conversely, as they are more linearly responsive to increases in autumn/winter rainfall, and less influenced by interseasonal storage dynamics, systems characterized as runoff-dominated (lower BFI) are more sensitive to wetter winters (i.e., increased amplitude). In these catchments baseflow makes a lesser contribution to total outflow, and precipitation events are more likely to generate direct/quick overland and shallow subsurface flow.

This is compounded by the fact that many peak flows occur during January and December in Ireland (~20–30% of all peaks annually). Consequently, in cases where total annual precipitation decreases but an increase in seasonality is experienced, catchments in clusters (d) and (e) are more likely to return an increase in flood magnitude.

Information on the hydrological signatures associated with each catchment is given in Figure 3 and Table S2. The BFI quantifies the long-term ratio of baseflow to total flow and is an important attribute when characterizing flood regime type. The index is a measure of the attenuated contribution to total discharge and is indicative of storage effects. Clusters (a) and (e) sit at opposing ends of the sensitivity spectrum and have BFI values (a: <0.4; e: >0.6) that characterize them (in relative terms) as groundwater and runoff-dominated systems, respectively. The greater baseflow influence in cluster (a) suggests these catchments have a longer memory. The greater influence of memory is also demonstrated by the higher correlation in month to month variations (1-month lag range: 0.14–0.55; 3-month lag range: 0–0.27) for cluster (a). Further assessment of the hydrological signatures shows that cluster (e) catchments have a higher RC and greater mean annual discharge (mm/year). In relation to high flow signatures this cluster is also associated with more frequent (high pulse count) and variable flow peaks (coefficient of variation and high flow variability). The significance of the annual water balance in influencing catchment response to a climate signal is highlighted by the prominence of the RC in differentiating sensitivity, ranging from 0.52 to 0.75 for clusters (a) and (e), respectively. RC is considered a measure of annual evaporative losses. Catchments with a lower RC also tend to be those with the lowest precipitation totals. This suggests that in dry catchments, summer soil moisture and storage deficits influence recharge capacity during wetter seasons, leading to reduced sensitivity to an increasingly seasonal precipitation regime.

3.3.4. Random Forest: Catchment Classification

Effective precipitation (variability, seasonality, and frequency/magnitude of extremes) and catchment properties (morphology, geology, soil cover, and land use type) interact to shape hydrological processes and function at different scales and ultimately influence flood sensitivity. Hence, using ensemble modeling to
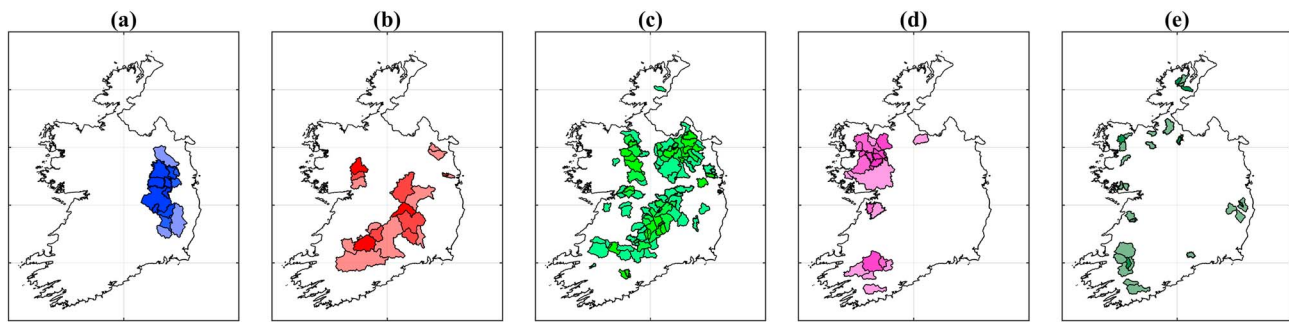
Figure 8. Classification of 215 catchments from the Flood Studies Update into one of five response types (a–e) using the random forest classifier.

establish a link between class membership of distinct sensitivity types and PCDs allows inferences to be made about the expected response of ungauged or data-sparse catchments.

Figure 8 displays the outcome of applying the RF (section 2.7) classifier in predictive mode using all (215) catchments for which PCDs (Table 1) are available. Figure 9 shows the misclassification probability for the OOB samples across the ensemble. It indicates the extent to which the model error stabilizes as the number of trees grown increases. The RF classifier is also used to investigate which attributes contribute most to prediction accuracy, and thus have the greatest explanatory power in differentiating sensitivity type. Figure 9 displays the PCDs according to their standardized importance score. The six most important predictors include: SAAR, BFIsoil, TAYSLO, PEAT, FLATWET, and MSL. Their values for the 215 catchments, discretized according to the predicted sensitivity type, are also shown in Figure 9.

Generally, the spatial pattern of the reduced sample (Figure 7) is reproduced, with west-east and upland-lowland gradients. The most important predictor is SAAR, which distinguishes between clusters based on annual precipitation total. Wetter/drier catchments are classified as more/less sensitive. Sensitivity class reflects the southwest to north/northeast gradient in precipitation totals across the Island. Generally, clusters (d–e) are located in upland and/or westerly locations with greater rainfall. Clusters (b and c) are representative of drier catchments in the Midlands. Finally, catchments from cluster (a) are the driest and are situated along the east coast. However, precipitation zones are correlated with a number of other features which may also influence sensitivity, including elevation, proximity to the coast, aspect, and soil type, none of which are represented by the PCDs or captured more distinctly by the catchment sample.

The importance of the BFI means a distinction is made between runoff and groundwater-dominated systems. Generally, catchments in clusters (a) and (e) sit at opposing ends of the BFI spectrum, with the former/latter having a higher/lower baseflow contribution. Clusters (d) and (e) have the highest proportion of peat (PEAT) coverage. They also have the largest values for FLATWET, indicating that soil moisture remains high for prolonged periods. This reflects the greater coverage of poorly draining soils in upland areas, the effect of which is to heighten flood sensitivity to heavy rainfall events. Mainstream length (MSL) is generally greatest for type (a) reflecting the more slowly draining nature of larger catchments located in the northeast. A distinction between the lowland- and upland-type systems is reiterated by TAYSLO. Here slope is generally greatest for catchment type (e) underlining their upland characteristics. Of the remaining predictors, potential evapotranspiration (SAAPE), stream frequency (STMFRQ), arterial drainage (ARTDRAIN2), and forest (FOREST) coverage are among the least important. Figure S9 shows the posterior probability of the sensitivity type assigned to each of the 215 catchments by the RF classifier. It demonstrates RF's utility for associating a measure of uncertainty with the classification.

3.4. Catchment Exposure to Future Climate

Figure 10 shows the combined exposure of all 215 catchments to future climate based on the CMIP5 ensemble. Catchments are classified into one of five sensitivity types according to their PCDs. The percent of EMs that exceed climate change allowances of 0% to 40% relative to baseline conditions are estimated using the centroid response surface for each cluster or corresponding sensitivity type (Figure 7). Hence, the mean response surface for clusters identified from the catchment sample (35) are assumed representative of catchments with similar characteristics within the larger (215) set.
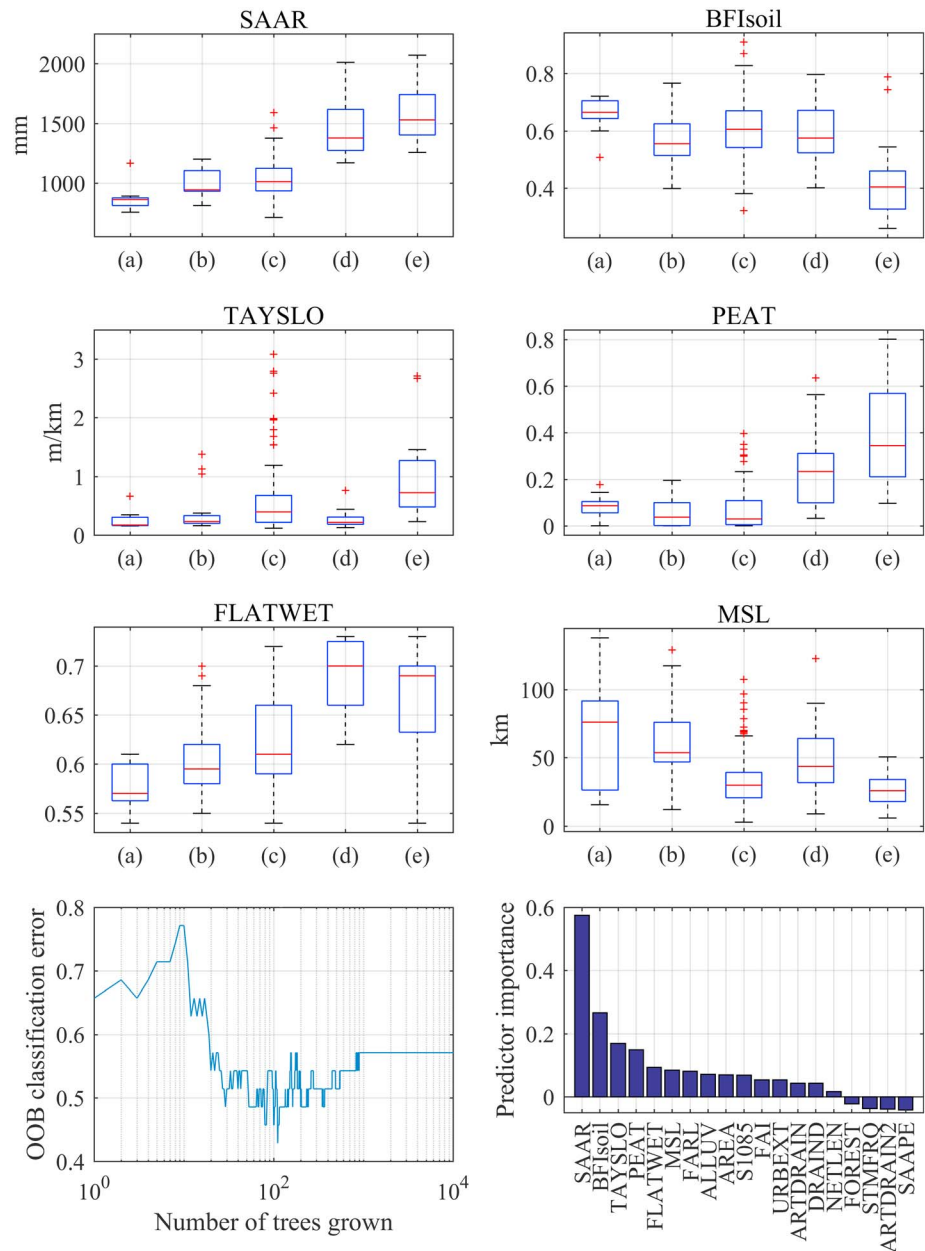
Figure 9. The "out-of-bag" misclassification probability plotted against the number of ensemble Classification Trees (lower left panel). Physical catchment descriptors ranked according to their standardized measure of importance (*y* axis; lower right panel). Boxplots showing the six most important physical catchment descriptors (SAAR, BFIsoil, TAYSLO, PEAT, FLATWET, and MSL) for the 215 catchments discretized into sensitivity type (a–e) using the random forest classifier. Boxplots show the median (central mark; q2) along with the 25th (bottom; q1) and 75th (top edges; q3) percentiles. Whiskers extend to q2 ± 1.57(q3 − q1)/sqrt(o) where o is the number of observations. Please refer to Table 1 for descriptions/definitions of SAAR, BFIsoil, TAYSLO, PEAT, FLATWET, and MSL.

The upper row in Figure 10 highlights exposure when projected changes for all RCPs and middle to late century horizons are considered. The 20% allowance is shown to offer protection against ~57% to 92% (~55% to 100%) of uncertainty in the CMIP5_Sub (CMIP5) ensemble. Results highlight the extent to which exposure varies for the same threshold across the five types and illustrates, as in the case of cluster (e), instances where a universally applied allowance of 20% may lead to overadaptation. Conversely, as illustrated by type (a), adoption of a 30% allowance may be necessary to provide an equivalent level of protection against future risk (as measured by the percent of ensemble accommodated). Variations in the level of exposure between types
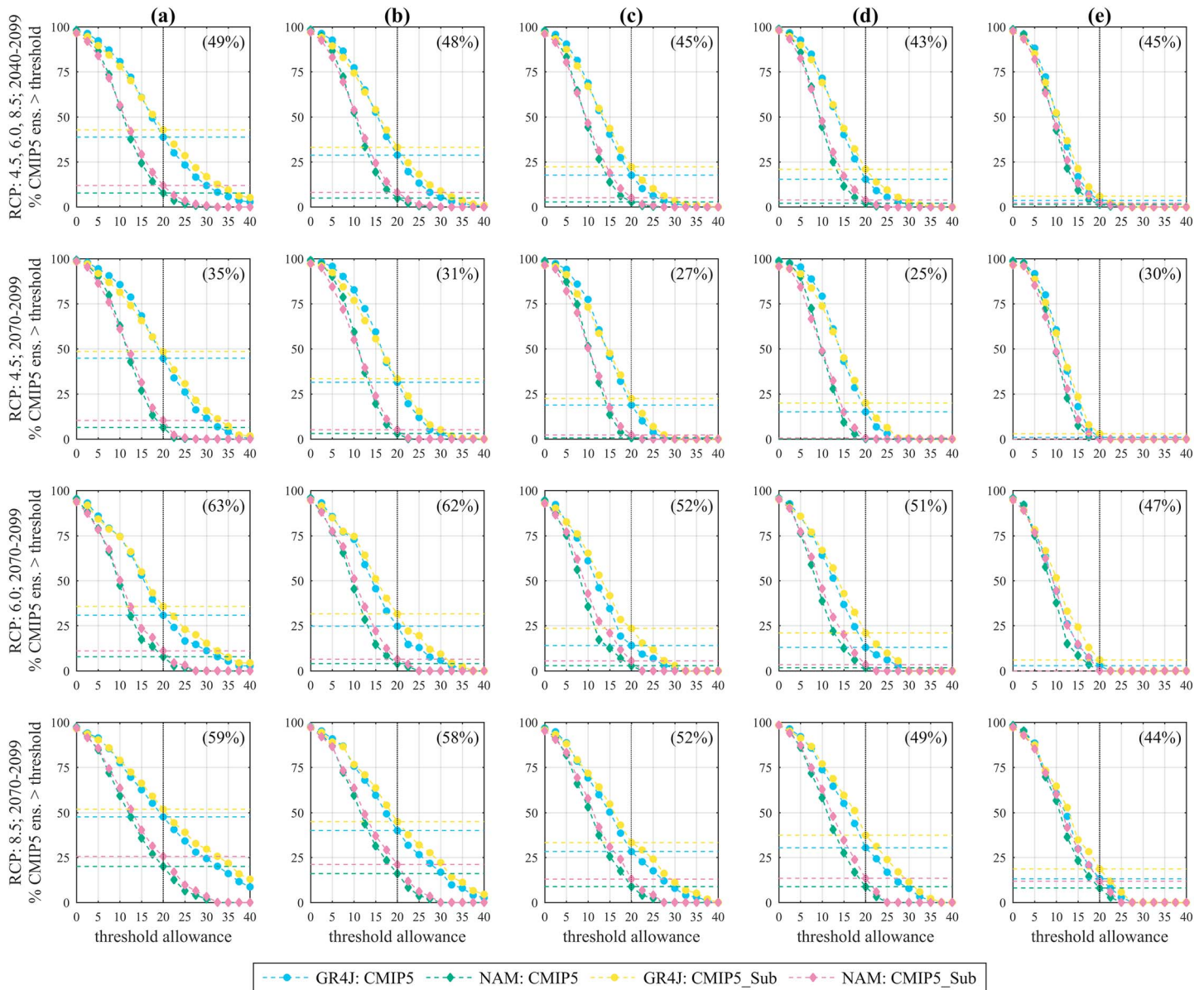
Figure 10. Percent of CMIP5 and CMIP5_Sub ensemble members (*y* axis) which exceed climate change allowances of 0–40% (relative to baseline conditions; *x* axis) calculated for each sensitivity type and hydrological model. The percent flood response and associated exposure is estimated using projections for all 215 catchments and the corresponding centroid relating to their sensitivity type. Plots show the exposure of each to projected climate and the adequacy of different adaptive capacity thresholds. The indicative 20% allowance is highlighted using the vertical black line. Combined threshold exceedances calculated for RCP4.5, RCP6, and RCP8.5 over the 2050s (2040–2069) and 2080s (2070–2099) are shown in the upper row. The second, third, and fourth rows show exceedances for the 2080s relating to RCP4.5, RCP6, and RCP8.5, respectively. The percent of the original CMIP5 ensemble members included in the CMIP5_Sub set is shown in brackets. RCP = Representative Concentration Pathways; CMIP5 = Coupled Model Intercomparison Project Phase 5.

generally follow the ranking of centroids from most to least sensitive (Table 2). Irrespective of the time horizon and RCP considered, results indicate that type (a)/(e) is most/least exposed. This can be attributed to the greater sensitivity of type (a) particularly to changes in mean annual precipitation. Given the marked response of type (d) to increases in seasonality, its exposure generally increases relative to types (b) and (c), particularly as changes in amplitude become more pronounced over successive time horizons and RCPs.

The subselected CMIP5 ensemble indicates similar exposure levels to those derived using the full ensemble—albeit that exposure for CMIP5_Sub is generally greater. This is despite the ensemble being notably

reduced in size. For example, dependent on RCP, sensitivity class and horizon, Figure 10 indicates a reduction of between 73% and 48% in ensemble size. The similarity in exposure, despite such reductions in size, is indicative of the scale of data redundancy. It is also noted that uncertainty from the hydrological models far exceeds uncertainty related to the use of CMIP5_Sub versus the full ensemble.

Figure 10 shows the extent of uncertainty due to hydrological model structure. Generally, there is close agreement between models for catchment type (e). In this case, each has a similar centroid response surface (Figure 7) and level of exposure across exceedance thresholds (Figure 10). However, for types (a)–(d) GR4J shows greater exposure relative to NAM. This is most pronounced for type (a) where differences in protection afforded by a 20% allowance differs by ~25% to 50% dependent on the RCP and time horizon. Although models disagree about the exact percentage exposure within individual types, each agrees as to the relative exposure between groups, with type (a)/(e) being the most/least exposed according to the 20% threshold. Given that the study examines changes in the seasonal amplitude of precipitation, along with the various dissimilarities in rainfall-runoff model structure, differences in the representation of antecedent conditions are (in part) causal to the models returning such different estimates of risk exposure.

4. Discussion

Although the chosen catchments provide good coverage of hydroclimatological variability across the island, the sample is limited in size with underrepresentation of small "flashy" systems, particularly along the western seaboard and uplands. By focusing on rivers with minimal artificial influences, heavily modified catchments such as those with regulated flows or large urban areas are excluded. This has important implications for study robustness, particularly relating to the clustering and discriminant analysis, wherein a larger sample would facilitate additional testing and may reduce noise allowing clearer identification of more distinct sensitivity types. The strength of the inferences drawn from both the importance of underlying physical processes and the extent to which results can be robustly generalized is also related to sample size and diversity. Similarly, the constraints posed by the list of available PCDs must be considered. It is possible that descriptors that better distinguish catchment type or provide a clearer indication of the hydrological processes at work are not included. Despite shortcomings the FSU provides an ideal starting point for developing a national set of PCDs (Mills et al., 2014). With the aim of improving regionalization, it is recommended that this data set is developed to include additional descriptors.

Using minimally affected catchments means that it is easier to elucidate the physical catchment controls (e.g., land cover, soil type, and morphometric attributes) on flood response, the absence of urbanized catchments (>10%) is also due to a lack of monitoring in these areas and their uniqueness in the Irish case. With respect to urban extent ~91% of the FSU (215) catchments have a similar urban coverage as the reduced catchment sample (~2% extent). Hence, results from our "natural" catchment sample are considered transferable to catchments with a small proportion (<5%) of urban extent.

Response surfaces are a powerful visual aid but they are limited to studying sensitivity along two (or maybe three) axes. This hinders graphical representation of changes for a larger set of climate parameters. The present analysis examined monthly scale changes, with results pointing to catchment memory and longer-term storage dynamics influencing sensitivity and risk exposure. However, small, catchments with a shorter memory and more linear rainfall-runoff response are also likely to be affected by changing patterns at (sub)daily scales, particularly for extreme events. Consequently, given a wider range of possible climate changes, the resultant classification reflects only one component in the overall picture of flood sensitivity for Ireland.

On the other hand, monthly precipitation changes are more confidently represented by GCMs given their coarse spatial resolution. Although GCMs are capable of capturing changes in slowly responding and spatially homogenous elements of the regime, such as the seasonal cycle, their resolution constrains their ability to resolve finer-scale processes and topographical features required to capture extremes. Hence, the study focuses on exploring sensitivity to those aspects of the regime (total amount and seasonality) for which we have greater confidence in the likely direction of change. Similarly, there is an implicit assumption that the rainfall-runoff models provide an accurate proxy of catchment behavior even when applied to climate conditions which differ greatly from the observations available for model development (Broderick et al., 2016).

Despite the pattern of response being similar between models, the study highlights the notable effect that structural differences in hydrological model have on flood estimates. This uncertainty has important implications for how response surfaces are interpreted and used for adaptation planning. Furthermore, it underlines the importance of addressing this aspect of uncertainty, particularly given the potential to underestimate true risk. It is shown, for example, that exposure across various thresholds within sensitivity types is greater for GR4J than NAM. Design decisions based on GR4J would require greater climate change allowances than those associated with NAM. We also focused on changes in the 20-year return period event. Rainfall-runoff model uncertainty would be expected to increase for more extreme floods, yet information on these rarer events may be needed in high-risk situations. Managers must, therefore, consider hydrological model uncertainty when specifying climate change allowances for a given catchment type, return period, RCP scenario, and time in the future.

By allowing exploration of key uncertainties, multimodel and perturbed physics ensembles are essential for avoiding maladaptations (Clark et al., 2016). However, CMIP5 essentially constitutes an "ensemble of opportunity"—derived from imperfect sampling of available climate projections, with implications for the overrepresentation/underrepresentation of constituent GCM sensitivities and biases. This study highlighted the extent of redundancy in the ensemble, wherein using k-medoids clustering the number of members are reduced (>50%) in some cases considerably. This redundancy was greatest for simulations from the same GCM, wherein within-model dependencies increase as the climate change signal strengthens. However, results highlight that subsampling the ensemble had little effect on the exposure estimates—albeit that a slight increase in risk is associated with the subselected set. Despite this, to provide a more statistically robust estimate of risk, we argue that selection of EMs should be on an objective basis, designed to address data redundancies and model interdependence. In comparing sources of uncertainty, the choice of hydrological model structure has a much greater effect on exposure estimates than uncertainty relating to whether the subselected or complete CMIP5 ensemble is used.

With the above issues in mind, this study represents a first step toward national climate change allowances for infrastructure that could accommodate expected climate-driven changes in flood risk across Ireland. By highlighting how catchments are differentially affected by specified precipitation changes, these climate change allowances could be tailored to meet regional/local vulnerabilities. In places of heightened exposure this avoids underestimation of risk; conversely, in catchments with greater natural resilience, unnecessary investments may be avoided. For example, the greatest exposure is associated with sensitivity types (a) and (b) which relates to ~22% of the 215 catchments. These catchments are generally low-lying drier catchments located in the midlands and east. They are associated with greater storage and longer catchment "memory" and thus are more greatly affected by interseasonal and interannual variability. Here exposure varies between ~20% (NAM; b) and 52% (GR4J; a) for the end of the century under RCP8.5 CMIP5 and CMIP5_Sub. While 20% generally provides a good level of protection, for these catchment types a marginal shift in allowances to 30% could accommodate a larger proportion of uncertainty. Conversely, our results also highlight that applying a universal 20% allowance could in some cases lead to costly overadaptation. This is particularly relevant for sensitivity type (e) which encompasses ~15% of the 215 catchments. Type (e) generally has a "flashier" flow regime and is located in more exposed relatively wetter upland areas. Overall, our results support Bastola et al. (2011b), who identified the Boyne catchment (ID: 7012; Eastern Ireland) as the most sensitive to changes in flood magnitude. In this specific case, an allowance of greater than 40% is necessary to reduce exposure (~7% exposure based on RCP8.5 CMIP5_Sub for 2070–2099) to a level comparable with less sensitive catchments. It is noted that, although all catchments are relatively more sensitive to changes in mean annual precipitation as opposed to amplitude, when considered in its entirety, the CMIP5 ensembles suggest that significant changes in seasonality are more likely. Hence, it cannot be assumed that greater sensitivity in one parameter is necessarily indicative of exposure to climate risk. This highlights the value of using climate ensemble alongside response surfaces.

Our results relating to the physical controls on flood response are commensurate with previous studies which highlight that, while rainfall quantities immediately preceding or during a flood event contribute to its magnitude, given the nonlinear nature of generating processes, the magnitude of antecedent storage (e.g., groundwater and soil moisture levels) is critical in preconditioning the catchment, and thus affect the frequency and scale of flood events across different time scales (Sivapalan et al., 2005; Ye et al., 2017).

Hence, a physically sensible relationship exists between the harmonic (mean and amplitude) parameters of annual precipitation explored here and changes in flood regimes.

5. Conclusions

This study implements a scenario-neutral framework as part of a national assessment of climate change allowances for flood risk under prescribed changes in the mean and seasonality of annual precipitation for Ireland. A typology of catchment sensitivities was established from which inferences can be made about the hydroclimatolgcial properties that influence sensitivity to climate change. A set of decision rules (based on easily derived physical catchment descriptors) was then used to regionalize sensitivity type to a wider catchment sample, including ungauged or data-sparse catchments. The study identified five sensitivity types, each associated with a distinct response pattern. Discriminant analysis revealed that (among the variables tested) annual precipitation, river channel slope, drainage density, and alluvial deposits are key predictors of sensitivity to climate-driven flood responses. Our results also highlight the notable effect of hydrological model structure on flood magnitude and hence the evaluation of catchment sensitivity to climate changes.

Our findings demonstrate the valuable insights into climate sensitivity that can be achieved for individual or regionalized catchment types using a scenario-neutral framework. Our approach provides a rigorous method for stress-testing adaptation decisions—in this case implementation of national or catchment-type climate change allowances for flood design or scenario definition. By exploring the sensitivity of additional design allowances to uncertainty within the CMIP5 climate model ensemble and two hydrological models, we show that for all five catchment types identified, a national climate change allowance of 20% caters for ~64% of the CMIP5_Sub ensemble spread (RCP8.5; 2070–2099). Conversely, a 10% allowance covers only ~27% of the same ensemble. In some instances, marginal increases of design allowances to 30% would offer greater protection, particularly given the uncertainties inherent to future flood risk estimation. Further research is needed to more thoroughly characterize these uncertainties. This applies especially in the case of hydrological model parametric uncertainty. Given its potential effects (particularly in simulating high flows), integrating this component of model uncertainty in the SN framework would provide a more robust estimate of risk exposure (Bastola et al., 2011b). In this respect, results should be treated with a degree of caution. Further research is also required to examine catchment sensitivity and exposure to short-duration (sub-daily) extreme rainfall events alongside seasonal/annual changes.

Given variations in exposure and sensitivity between catchment types, we assert that a national allowance could lead to overadaptation and potential misdirection of flood defense funds in some cases. This is because some catchments have greater natural resilience and, according to the CMIP5 ensemble, are less exposed to future flood risk. Under these circumstances, a 20% allowance may be too precautionary. Hence, we advocate a more targeted, risk-based approach whereby the sensitivity of individual catchment types is used to prioritize investment. The study highlights the importance of managing climate change risk on the basis of catchment type rather than region or administrative boundary. It is recognized that spatial proximity cannot always be assumed the best predictor of hydrological similarity (Merz & Blöschl, 2005). Hence, any future "lookup" table of allowances should really be structured by catchment type rather than region (Reynard et al., 2017). Our framework is applicable to other national contexts where authorities are also seeking to establish allowances for climate change that balance the costs of increased standards of protection versus the amount of uncertainty in future flood risk that can be accommodated.

References

Ahilan, S., O'Sullivan, J. J., & Bruen, M. (2012). Influences on flood frequency distributions in Irish river catchments. *Hydrology and Earth System Sciences*, *16*(4), 1137–1150. https://doi.org/10.5194/hess-16-1137-2012

Anandhi, A., Frei, A., Pierson, D. C., Schneiderman, E. M., Zion, M. S., Lounsbury, D., & Matonse, A. H. (2011). Examination of change factor methodologies for climate change impact assessment. *Water Resources Research*, *47*, W03501. https://doi.org/10.1029/2010WR009104

Andréassian, V., Coron, L., Lerat, J., & Le Moine, N. (2016). Climate elasticity of streamflow revisited—An elasticity index based on long-term hydrometeorological records. *Hydrology and Earth System Sciences*, *20*(11), 4503–4524. https://doi.org/10.5194/hess-20-4503-2016

Bastola, S., Murphy, C., & Fealy, R. (2012). Generating probabilistic estimates of hydrological response for Irish catchments using a weather generator and probabilistic climate change scenarios. *Hydrological Processes*, *26*(15), 2307–2321. https://doi.org/10.1002/hyp.8349

Bastola, S., Murphy, C., & Sweeney, J. (2011a). The role of hydrological modelling uncertainties in climate change impact assessments of Irish river catchments. *Advances in Water Resources*, *34*(5), 562–576. https://doi.org/10.1016/j.advwatres.2011.01.008

Bastola, S., Murphy, C., & Sweeney, J. (2011b). The sensitivity of fluvial flood risk in Irish catchments to the range of IPCC AR4 climate change scenarios. *Science of the Total Environment*, *409*(24), 5403–5415. https://doi.org/10.1016/j.scitotenv.2011.08.042

Beven, K. (2006). A manifesto for the equifinality thesis. *Journal of Hydrology*, *320*(1–2), 18–36. https://doi.org/10.1016/j.jhydrol.2005.07.007

Beven, K., & Binley, A. (1992). The future of distributed models: Model calibration and uncertainty prediction. *Hydrological Processes*, *6*(3), 279–298. https://doi.org/10.1002/hyp.3360060305

Beven, K., & Binley, A. (2014). GLUE: 20 years on. *Hydrological Processes*, *28*(24), 5897–5918. https://doi.org/10.1002/hyp.10082

Booker, D. J., & Woods, R. A. (2014). Comparing and combining physically-based and empirically-based approaches for estimating the hydrology of ungauged catchments. *Journal of Hydrology*, *508*, 227–239. https://doi.org/10.1016/j.jhydrol.2013.11.007

Breiman, L. (1996). Bagging predictors. *Machine Learning*, *24*(2), 123–140. https://doi.org/10.1007/BF00058655

Breiman, L. (2001). Random forests. *Machine Learning*, *45*(1), 5–32. https://doi.org/10.1023/A:1010933404324

Broderick, C., Matthews, T., Wilby, R. L., Bastola, S., & Murphy, C. (2016). Transferability of hydrological models and ensemble averaging methods between contrasting climatic periods. *Water Resources Research*, *52*, 8343–8373. https://doi.org/10.1002/2016WR018850

Brown, C. (2011). *Decision-scaling for robust planning and policy under climate uncertainty*, *World Resources Report Uncertainty Series* (p. 14). Washington, DC: World Resources Institute.

Brown, C., Ghile, Y., Laverty, M., & Li, K. (2012). Decision scaling: Linking bottom-up vulnerability analysis with climate projections in the water sector. *Water Resources Research*, *48*, W09537. https://doi.org/10.1029/2011WR011212

Brown, C., Werick, W., Leger, W., & Fay, D. (2011). A decision-analytic approach to managing climate risks: Application to the upper Great Lakes 1: A decision-analytic approach to managing climate risks: Application to the upper Great Lakes. *JAWRA Journal of the American Water Resources Association*, *47*(3), 524–534. https://doi.org/10.1111/j.1752-1688.2011.00552.x

Brown, C., & Wilby, R. L. (2012). An alternate approach to assessing climate risks. *Eos, Transactions American Geophysical Union*, *93*(41), 401–402.

Bussi, G., Dadson, S. J., Prudhomme, C., & Whitehead, P. G. (2016). Modelling the future impacts of climate and land-use change on suspended sediment transport in the River Thames (UK). *Journal of Hydrology*, *542*, 357–372. https://doi.org/10.1016/j.jhydrol.2016.09.010

Bussi, G., Whitehead, P. G., Bowes, M. J., Read, D. S., Prudhomme, C., & Dadson, S. J. (2016). Impacts of climate change, land-use change and phosphorus reduction on phytoplankton in the River Thames (UK). *Science of the Total Environment*, *572*, 1507–1519. https://doi.org/10.1016/j.scitotenv.2016.02.109

Calinski, T., & Harabasz, J. (1974). A dendrite method for cluster analysis. *Communications in Statistics - Theory and Methods*, *3*(1), 1–27. https://doi.org/10.1080/03610927408827101

Cameron, D. S., Beven, K. J., Tawn, J., Blazkova, S., & Naden, P. (1999). Flood frequency estimation by continuous simulation for a gauged upland catchment (with uncertainty). *Journal of Hydrology*, *219*(3), 169–187.

Cannon, A. J. (2015). Selecting GCM scenarios that span the range of changes in a multimodel ensemble: Application to CMIP5 climate extremes indices*. *Journal of Climate*, *28*(3), 1260–1267. https://doi.org/10.1175/JCLI-D-14-00636.1

Chen, J., Brissette, F. P., & Leconte, R. (2012). WeaGETS—A Matlab-based daily scale weather generator for generating precipitation and temperature. *Procedia Environmental Sciences*, *13*, 2222–2235. https://doi.org/10.1016/j.proenv.2012.01.211

Chen, J., Brissette, F. P., & Leconte, R. (2010). A daily stochastic weather generator for preserving low-frequency of climate variability. *Journal of Hydrology*, *388*(3–4), 480–490. https://doi.org/10.1016/j.jhydrol.2010.05.032

Chiew, F. H. S. (2006). Estimation of rainfall elasticity of streamflow in Australia. *Hydrological Sciences Journal*, *51*(4), 613–625. https://doi.org/10.1623/hysj.51.4.613

Clark, M. P., Kavetski, D., & Fenicia, F. (2011). Pursuing the method of multiple working hypotheses for hydrological modeling: Hypothesis testing in hydrology. *Water Resources Research*, *47*, W09301. https://doi.org/10.1029/2010WR009827

Clark, M. P., Wilby, R. L., Gutmann, E. D., Vano, J. A., Gangopadhyay, S., Wood, A. W., et al. (2016). Characterizing uncertainty of the hydrologic impacts of climate change. *Current Climate Change Reports*, *2*(2), 55–64. https://doi.org/10.1007/s40641-016-0034-x

Culley, S., Noble, S., Yates, A., Timbs, M., Westra, S., Maier, H. R., et al. (2016). A bottom-up approach to identifying the maximum operational adaptive capacity of water resource systems to a changing climate. *Water Resources Research*, *52*, 6751–6768. https://doi.org/10.1002/2015WR018253

DCLG (2012). *Technical guidance to the national planning policy framework*. London: Department for Communities and Local Government.

Déqué, M., & Somot, S. (2010). Weighted frequency distributions express modelling uncertainties in the ENSEMBLES regional climate experiments. *Climate Research*, *44*(2–3), 195–209. https://doi.org/10.3354/cr00866

Diaz-Nieto, J., & Wilby, R. L. (2005). A comparison of statistical downscaling and climate change factor methods: Impacts on low flows in the River Thames, United Kingdom. *Climatic Change*, *69*(2), 245–268.

Dooge, J. C. I., Bruen, M., & Parmentier, B. (1999). A simple model for estimating the sensitivity of runoff to long-term changes in precipitation without a change in vegetation. *Advances in Water Resources*, *23*(2), 153–163.

Ekström, M., Gutmann, E. D., Wilby, R. L., Tye, M. R., & Kirono, D. G. C. (2018). Robustness of hydroclimate metrics for climate change impact research. *Wiley Interdisciplinary Reviews Water*, *5*(4), e1288. https://doi.org/10.1002/wat2.1288

Fu, G., Charles, S. P., & Chiew, F. H. S. (2007). A two-parameter climate elasticity of streamflow index to assess climate change effects on annual streamflow. *Water Resources Research*, *43*, W11419. https://doi.org/10.1029/2007WR005890

Ghile, Y. B., Taner, M. ü., Brown, C., Grijsen, J. G., & Talbi, A. (2014). Bottom-up climate risk assessment of infrastructure investment in the Niger River basin. *Climatic Change*, *122*(1–2), 97–110. https://doi.org/10.1007/s10584-013-1008-9

Government of Ireland (2018). Project Ireland 2040 national development plan 2018–2027. Department of Public Expenditure and Reform.

Greene, A. M., Goddard, L., & Lall, U. (2006). Probabilistic multimodel regional temperature change projections. *Journal of Climate*, *19*(17), 4326–4343.

Guo, D., Westra, S., & Maier, H. R. (2017). Use of a scenario-neutral approach to identify the key hydro-meteorological attributes that impact runoff from a natural catchment. *Journal of Hydrology*, *554*, 317–330. https://doi.org/10.1016/j.jhydrol.2017.09.021

Harrison, S. P., Bartlein, P. J., Izumi, K., Li, G., Annan, J., Hargreaves, J., et al. (2015). Evaluation of CMIP5 palaeo-simulations to improve climate projections. *Nature Climate Change*, *5*(8), 735–743. https://doi.org/10.1038/nclimate2649

Hastie, T., Tibshirani, S., & Friedman, H. (2009). *The elements of statistical learning* (2nd ed.). New York: Springer.

Hrachowitz, M., Fovet, O., Ruiz, L., Euser, T., Gharari, S., Nijzink, R., et al. (2014). Process consistency in models: The importance of system signatures, expert knowledge, and process complexity. *Water Resources Research*, *50*, 7445–7469. https://doi.org/10.1002/2014WR015484

Juhola, S., Glaas, E., Linnér, B.-O., & Neset, T.-S. (2016). Redefining maladaptation. *Environmental Science & Policy*, *55*, 135–140. https://doi.org/10.1016/j.envsci.2015.09.014

Katsavounidis, I., Jay Kuo, C.-C., & Zhang, Z. (1994). A new initialization technique for generalized Lloyd iteration. *IEEE Signal Processing Letters*, *1*(10), 144–146. https://doi.org/10.1109/97.329844

Kaufman, L., & Rousseeuw, P. J. (2005). *Finding groups in data: An introduction to Cluster analysis*. Hoboken, NJ: Wiley.

Kay, A. L., Bell, V. A., Blyth, E. M., Crooks, S. M., Davies, H. N., & Reynard, N. S. (2013). A hydrological perspective on evaporation: Historical trends and future projections in Britain. *Journal of Water and Climate Change*, *4*(3), 193. https://doi.org/10.2166/wcc.2013.014

Kay, A. L., Crooks, S. M., Davies, H. N., Prudhomme, C., & Reynard, N. S. (2014). Probabilistic impacts of climate change on flood frequency using response surfaces I: England and Wales. *Regional Environmental Change*, *14*(3), 1215–1227. https://doi.org/10.1007/s10113-013-0563-y

Kay, A. L., Crooks, S. M., Davies, H. N., & Reynard, N. S. (2014). Probabilistic impacts of climate change on flood frequency using response surfaces II: Scotland. *Regional Environmental Change*, *14*(3), 1243–1255. https://doi.org/10.1007/s10113-013-0564-x

Kay, A. L., Crooks, S. M., & Reynard, N. S. (2014). Using response surfaces to estimate impacts of climate change on flood peaks: Assessment of uncertainty. *Hydrological Processes*, *28*(20), 5273–5287. https://doi.org/10.1002/hyp.10000

Kendon, E. J., Rowell, D. P., Jones, R. G., & Buonomo, E. (2008). Robustness of future changes in local precipitation extremes. *Journal of Climate*, *21*(17), 4280–4297. https://doi.org/10.1175/2008JCLI2082.1

Knutti, R., Masson, D., & Gettelman, A. (2013). Climate model genealogy: Generation CMIP5 and how we got there. *Geophysical Research Letters*, *40*, 1194–1199. https://doi.org/10.1002/grl.50256

Köplin, N., Schädler, B., Viviroli, D., & Weingartner, R. (2012). Relating climate change signals and physiographic catchment properties to clustered hydrological response types. *Hydrology and Earth System Sciences*, *16*(7), 2267–2283. https://doi.org/10.5194/hess-16-2267-2012

Lin, Y., Dong, W., Zhang, M., Xie, Y., Xue, W., Huang, J., & Luo, Y. (2017). Causes of model dry and warm bias over central U.S. and impact on climate projections. *Nature Communications*, *8*(1). https://doi.org/10.1038/s41467-017-01040-2

Lloyd, S. (1982). Least squares quantization in PCM. *IEEE Transactions on Information Theory*, *28*(2), 129–137.

Löschner, L., Herrnegger, M., Apperl, B., Senoner, T., Seher, W., & Nachtnebel, H. P. (2017). Flood risk, climate change and settlement development: A micro-scale assessment of Austrian municipalities. *Regional Environmental Change*, *17*(2), 311–322. https://doi.org/10.1007/s10113-016-1009-0

Madsen, H. (2000). Automatic calibration of a conceptual rainfall–runoff model using multiple objectives. *Journal of Hydrology*, *235*(3), 276–288.

Mantovan, P., & Todini, E. (2006). Hydrological forecasting uncertainty assessment: Incoherence of the GLUE methodology. *Journal of Hydrology*, *330*(1–2), 368–381. https://doi.org/10.1016/j.jhydrol.2006.04.046

Maraun, D., Shepherd, T. G., Widmann, M., Zappa, G., Walton, D., Gutiérrez, J. M., et al. (2017). Towards process-informed bias correction of climate change simulations. *Nature Climate Change*, *7*(11), 664–773. https://doi.org/10.1038/nclimate3418

Masson, D., & Knutti, R. (2011). Climate model genealogy. *Geophysical Research Letters*, *38*, L08703. https://doi.org/10.1029/2011GL046864

Matthews, T., Murphy, C., McCarthy, G., Broderick, C., & Wilby, R. L. (2018). Super storm Desmond: A process-based assessment. *Environmental Research Letters*, *13*(1), 014024. https://doi.org/10.1088/1748-9326/aa98c8

McKay, M. D., Beckman, R. J., & Conover, W. J. (1979). A comparison of three methods for selecting values of input variables in the analysis of output from a computer code. *Technometrics*, *21*(2), 239. https://doi.org/10.2307/1268522

McMillan, H., Westerberg, I., & Branger, F. (2017). Five guidelines for selecting hydrological signatures. *Hydrological Processes*. https://doi.org/10.1002/hyp.11300

Mendlik, T., & Gobiet, A. (2016). Selecting climate simulations for impact studies based on multivariate patterns of climate change. *Climatic Change*, *135*(3–4), 381–393. https://doi.org/10.1007/s10584-015-1582-0

Merz, R., & Blöschl, G. (2005). Flood frequency regionalisation—Spatial proximity vs. catchment attributes. *Journal of Hydrology*, *302*(1–4), 283–306. https://doi.org/10.1016/j.jhydrol.2004.07.018

Mills, P., Nicholson, O., & Reed, D. (2014). Flood studies update technical research report (Volume IV. Physical catchment descriptors). Office of Public Works.

Mockler, E. M., O'Loughlin, F. E., & Bruen, M. (2016). Understanding hydrological flow paths in conceptual catchment models using uncertainty and sensitivity analysis. *Computers & Geosciences*, *90*, 66–77. https://doi.org/10.1016/j.cageo.2015.08.015

Murphy, C., Harrigan, S., Hall, J., & Wilby, R. L. (2013). HydroDetect: The identification and assessment of climate change indicators for an Irish reference network of river flow stations. Climate Change Research Programme (CCRP) 2007–2013 Report Series No. 27. ISBN 978-1-84095-507-1

Nash, J. E., & Sutcliffe, J. V. (1970). River flow forecasting through conceptual models part I — A discussion of principles. *Journal of Hydrology*, *10*(3), 282–290. https://doi.org/10.1016/0022-1694(70)90255-6

O'Callaghan, J., & David, M. (1984). The extraction of drainage networks from digital elevation data. *Computer Vision, Graphics, and Image Processing*, *28*(3), 22. https://doi.org/10.1016/S0734-189X(84)80011-0

OPW (2012). The national preliminary flood Risk assessment (PFRA) overview report. Office of Public Works.

OPW (2015). Draft climate change sectoral adaptation plan flood risk management (2015–2019). Office of Public Works.

Oudin, L., Hervieu, F., Michel, C., Perrin, C., Andréassian, V., Anctil, F., & Loumagne, C. (2005). Which potential evapotranspiration input for a lumped rainfall–runoff model? *Journal of Hydrology*, *303*(1–4), 290–306. https://doi.org/10.1016/j.jhydrol.2004.08.026

Pennell, C., & Reichler, T. (2011). On the effective number of climate models. *Journal of Climate*, *24*(9), 2358–2367. https://doi.org/10.1175/2010JCLI3814.1

Perez, J., Menendez, M., Mendez, F. J., & Losada, I. J. (2014). Evaluating the performance of CMIP3 and CMIP5 global climate models over the north-east Atlantic region. *Climate Dynamics*, *43*(9–10), 2663–2680. https://doi.org/10.1007/s00382-014-2078-8

Perrin, C., Michel, C., & Andréassian, V. (2003). Improvement of a parsimonious model for streamflow simulation. *Journal of Hydrology*, *279*(1–4), 275–289. https://doi.org/10.1016/S0022-1694(03)00225-7

Pirtle, Z., Meyer, R., & Hamilton, A. (2010). What does it mean when climate models agree? A case for assessing independence among general circulation models. *Environmental Science & Policy*, *13*(5), 351–361. https://doi.org/10.1016/j.envsci.2010.04.004

Poff, N. L., Brown, C. M., Grantham, T. E., Matthews, J. H., Palmer, M. A., Spence, C. M., et al. (2016). Sustainable water management under future uncertainty with eco-engineering decision scaling. *Nature Climate Change*, *6*(1), 25–34. https://doi.org/10.1038/nclimate2765

Prudhomme, C., Crooks, S., Kay, A. L., & Reynard, N. (2013). Climate change and river flooding: Part 1 Classifying the sensitivity of British catchments. *Climatic Change*, *119*(3–4), 933–948. https://doi.org/10.1007/s10584-013-0748-x

Prudhomme, C., Jakob, D., & Svensson, C. (2003). Uncertainty and climate change impact on the flood regime of small UK catchments. *Journal of Hydrology*, *277*(1–2), 1–23. https://doi.org/10.1016/S0022-1694(03)00065-9

Prudhomme, C., Kay, A. L., Crooks, S., & Reynard, N. (2013). Climate change and river flooding: Part 2 Sensitivity characterisation for British catchments and example vulnerability assessments. *Climatic Change*, *119*(3–4), 949–964. https://doi.org/10.1007/s10584-013-0726-3

Prudhomme, C., Sauquet, E., & Watts, G. (2015). Low flow response surfaces for drought decision support: A case study from the UK. *Journal of Extreme Events*, *02*(02), 1550005. https://doi.org/10.1142/S2345737615500050

Prudhomme, C., Wilby, R. L., Crooks, S., Kay, A. L., & Reynard, N. S. (2010). Scenario-neutral approach to climate change impact studies: Application to flood risk. *Journal of Hydrology*, *390*(3–4), 198–209. https://doi.org/10.1016/j.jhydrol.2010.06.043

Räisänen, J., & Ruokolainen, L. (2006). Probabilistic forecasts of near-term climate change based on a resampling ensemble technique. *Tellus A: Dynamic Meteorology and Oceanography*, *58*(4), 461–472. https://doi.org/10.1111/j.1600-0870.2006.00189.x

Reynard, N. S., Kay, A. L., Anderson, M., Donovan, B., & Duckworth, C. (2017). The evolution of climate change guidance for fluvial flood risk management in England. *Progress in Physical Geography*, *41*(2), 222–237. https://doi.org/10.1177/0309133317702566

Richardson, C. W. (1981). Stochastic simulation of daily precipitation, temperature, and solar radiation. *Water Resources Research*, *17*(1), 182–190. https://doi.org/10.1029/WR017i001p00182

Sankarasubramanian, A., Vogel, R. M., & Limbrunner, J. F. (2001). Climate elasticity of streamflow in the United States. *Water Resources Research*, *37*(6), 1771–1781. https://doi.org/10.1029/2000WR900330

Scussolini, P., Aerts, J. C. J. H., Jongman, B., Bouwer, L. M., Winsemius, H. C., de Moel, H., & Ward, P. J. (2016). FLOPROS: An evolving global database of flood protection standards. *Natural Hazards and Earth System Sciences*, *16*(5), 1049–1061. https://doi.org/10.5194/nhess-16-1049-2016

Singh, R., Wagener, T., Crane, R., Mann, M. E., & Ning, L. (2014). A vulnerability driven approach to identify adverse climate and land use change combinations for critical hydrologic indicator thresholds: Application to a watershed in Pennsylvania, USA. *Water Resources Research*, *50*, 3409–3427. https://doi.org/10.1002/2013WR014988

Sivapalan, M., Blöschl, G., Merz, R., & Gutknecht, D. (2005). Linking flood frequency to long-term water balance: Incorporating effects of seasonality. *Water Resources Research*, *41*, W06012. https://doi.org/10.1029/2004WR003439

Smith, K., Wilby, R., Broderick, C., Prudhomme, C., Matthews, T., Harrigan, S., & Murphy, C. (2018). Navigating cascades of uncertainty—As easy as ABC? Not quite. *Journal of Extreme Events*, 1850007. https://doi.org/10.1142/S2345737618500070

Snelder, T. H., Datry, T., Lamouroux, N., Larned, S. T., Sauquet, E., Pella, H., & Catalogne, C. (2013). Regionalization of patterns of flow intermittence from gauging station records. *Hydrology and Earth System Sciences*, *17*(7), 2685–2699. https://doi.org/10.5194/hess-17-2685-2013

Stedinger, J. R., Vogel, R. M., Lee, S. U., & Batchelder, R. (2008). Appraisal of the generalized likelihood uncertainty estimation (GLUE) method. *Water Resources Research*, *44*, W00B06. https://doi.org/10.1029/2008WR006822

Steinschneider, S., McCrary, R., Mearns, L. O., & Brown, C. (2015). The effects of climate model similarity on probabilistic climate projections and the implications for local, risk-based adaptation planning. *Geophysical Research Letters*, *42*, 5014–5044. https://doi.org/10.1002/2015GL064529

Steinschneider, S., Wi, S., & Brown, C. (2015). The integrated effects of climate and hydrologic uncertainty on future flood risk assessments. *Hydrological Processes*, *29*(12), 2823–2839. https://doi.org/10.1002/hyp.10409

Stephenson, D. B., Kumar, K. R., Doblas-Reyes, F. J., Royer, J.-F., Chauvin, F., & Pezzulli, S. (1999). Extreme daily rainfall events and their impact on ensemble forecasts of the Indian monsoon. *Monthly Weather Review*, *127*(9), 1954–1966. https://doi.org/10.1175/1520-0493(1999)127<1954:EDREAT>2.0.CO;2

Taylor, K. E., Stouffer, R. J., & Meehl, G. A. (2012). An overview of CMIP5 and the experiment design. *Bulletin of the American Meteorological Society*, *93*(4), 485–498. https://doi.org/10.1175/BAMS-D-11-00094.1

Turner, S. W. D., Marlow, D., Ekström, M., Rhodes, B. G., Kularathna, U., & Jeffrey, P. J. (2014). Linking climate projections to performance: A yield-based decision scaling assessment of a large urban water resources system. *Water Resources Research*, *50*, 3553–3567. https://doi.org/10.1002/2013WR015156

Vaze, J., Teng, J., & Chiew, F. H. S. (2011). Assessment of GCM simulations of annual and seasonal rainfall and daily rainfall distribution across south-east Australia. *Hydrological Processes*, *25*(9), 1486–1497. https://doi.org/10.1002/hyp.7916

Visessri, S., & McIntyre, N. (2016). Regionalisation of hydrological responses under land-use change and variable data quality. *Hydrological Sciences Journal*, *61*(2), 302–320. https://doi.org/10.1080/02626667.2015.1006226

Vormoor, K., Rössler, O., Bürger, G., Bronstert, A., & Weingartner, R. (2017). When timing matters-considering changing temporal structures in runoff response surfaces. *Climatic Change*, *142*(1–2), 213–226. https://doi.org/10.1007/s10584-017-1940-1

Walsh, S. (2012). Long term rainfall averages for Ireland. Presented at the National Hydrology Seminar, Tullamore, Ireland: Office of Public Works.

Wang, C., Zhang, L., Lee, S.-K., Wu, L., & Mechoso, C. R. (2014). A global perspective on CMIP5 climate model biases. *Nature Climate Change*, *4*(3), 201–205. https://doi.org/10.1038/nclimate2118

Weiß, M. (2011). Future water availability in selected European catchments: A probabilistic assessment of seasonal flows under the IPCC A1B emission scenario using response surfaces. *Natural Hazards and Earth System Sciences*, *11*(8), 2163–2171. https://doi.org/10.5194/nhess-11-2163-2011

Weiß, M., & Alcamo, J. (2011). A systematic approach to assessing the sensitivity and vulnerability of water availability to climate change in Europe. *Water Resources Research*, *47*, W02549. https://doi.org/10.1029/2009WR008516

Westerberg, I. K., Wagener, T., Coxon, G., McMillan, H. K., Castellarin, A., Montanari, A., & Freer, J. (2016). Uncertainty in hydrological signatures for gauged and ungauged catchments. *Water Resources Research*, *52*, 1847–1865. https://doi.org/10.1002/2015WR017635

Whateley, S., Steinschneider, S., & Brown, C. (2014). A climate change range-based method for estimating robustness for water resources supply. *Water Resources Research*, *50*, 8944–8961. https://doi.org/10.1002/2014WR015956

Wilby, R., Dawson, C., Murphy, C., O'Connor, P., & Hawkins, E. (2014). The Statistical DownScaling Model-Decision Centric (SDSM-DC): Conceptual basis and applications. *Climate Research*, *61*(3), 259–276. https://doi.org/10.3354/cr01254

Yang, C., Chandler, R. E., Isham, V. S., & Wheater, H. S. (2005). Spatial-temporal rainfall simulation using generalized linear models. *Water Resources Research*, *41*, W11415. https://doi.org/10.1029/2004WR003739

Yates, D. N., Miller, K. A., Wilby, R. L., & Kaatz, L. (2015). Decision-centric adaptation appraisal for water management across Colorado's continental divide. *Climate Risk Management*, *10*, 35–50. https://doi.org/10.1016/j.crm.2015.06.001

Ye, S., Li, H.-Y., Leung, L. R., Guo, J., Ran, Q., Demissie, Y., & Sivapalan, M. (2017). Understanding flood seasonality and its temporal shifts within the contiguous United States. *Journal of Hydrometeorology*, *18*(7), 1997–2009. https://doi.org/10.1175/JHM-D-16-0207.1